Physics and Applications of Metallic Magnetic Calorimeters

Loredana Gastaldo

Kirchhoff Institute for Physics
Heidelberg University

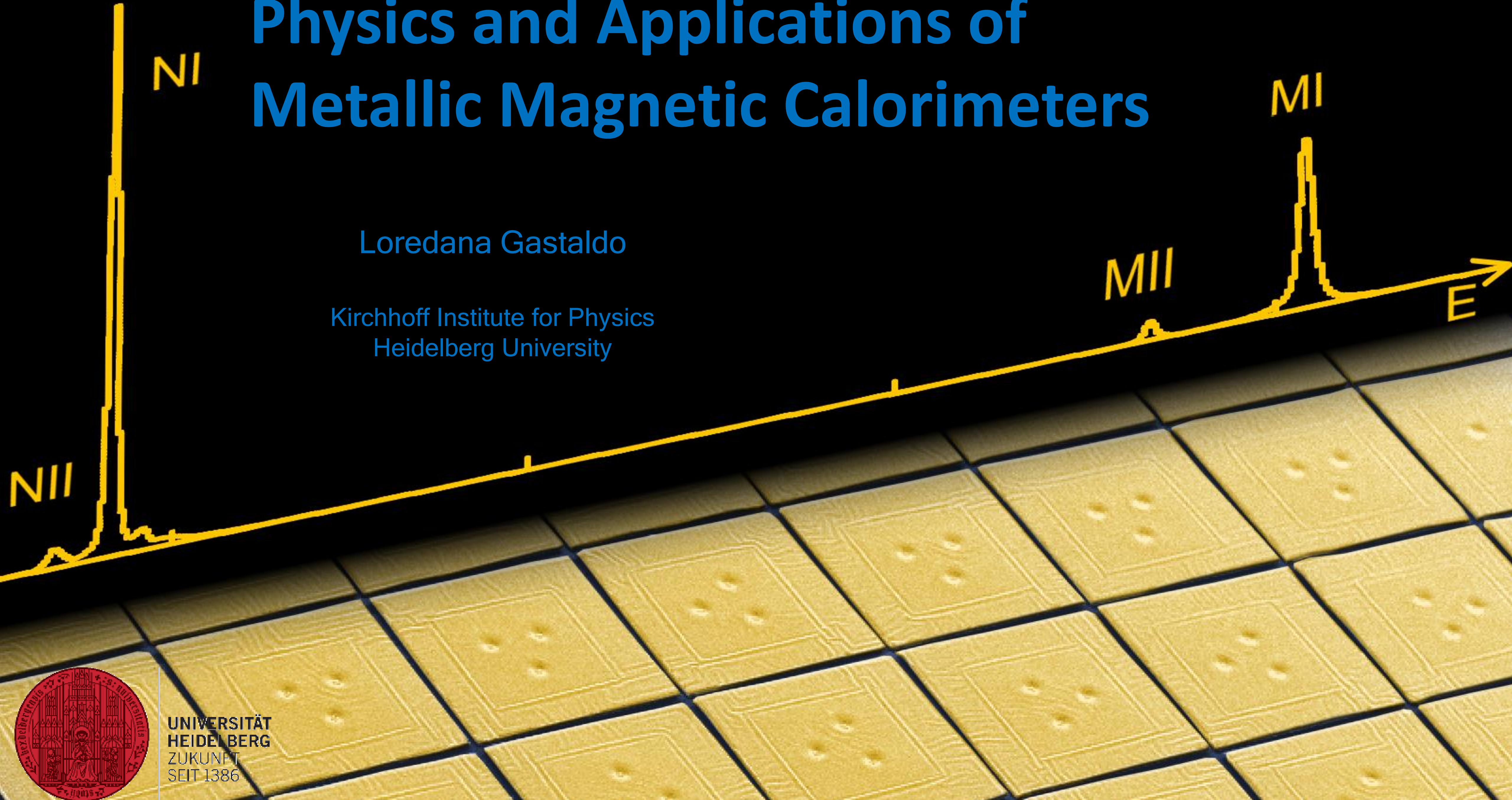

UNIVERSITÄT
HEIDELBERG
ZUKUNFT
SEIT 1386

Outline

- Metallic magnetic calorimeters
  - Thermodynamical properties
  - Readout
  - Fabrication
- MMC applications and performance
  - x-ray
  - Molecular fragments
  - Neutrino mass – ECHo
- Conclusions

Low Temperature Calorimeters

Near equilibrium detectors

Energy deposition induces increase of temperature

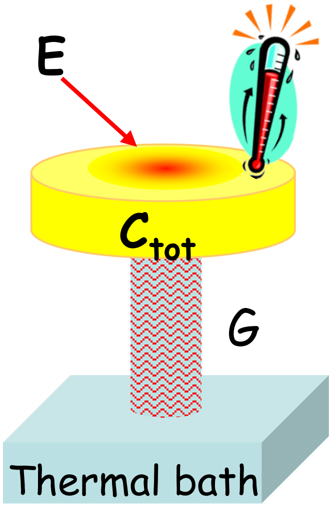

$$\Delta T \cong \frac{E}{C_{tot}}$$

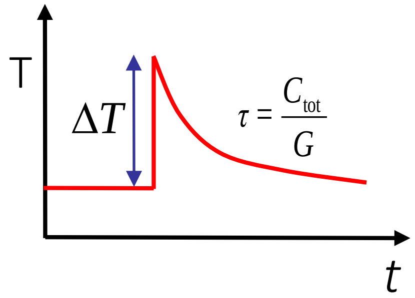

- Very small volume
- Working temperature below 100 mK

  small specific heat

  small thermal noise
- **Very sensitive temperature sensors**

Low Temperature Calorimeters

Near equilibrium detectors

Energy deposition induces increase of temperature

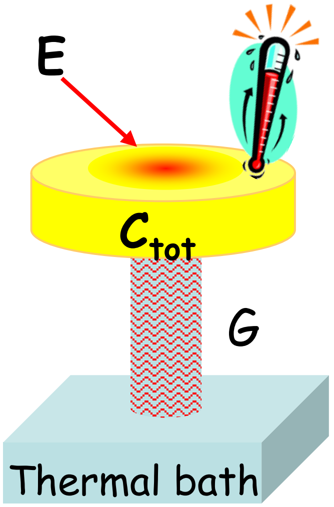

$$\Delta T \cong \frac{E}{C_{tot}}$$

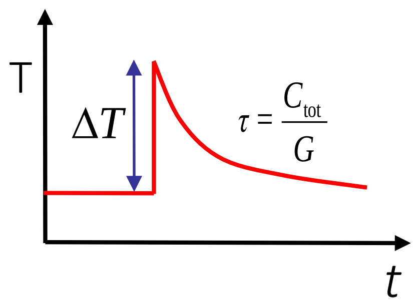

- Very small volume
- Working temperature below 100 mK
  - small specific heat
  - small thermal noise
- **Very sensitive temperature sensors**

Resistance of highly doped semiconductors

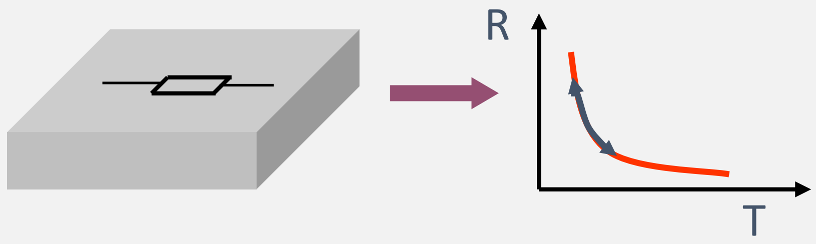

Resistance at superconducting transition,TES

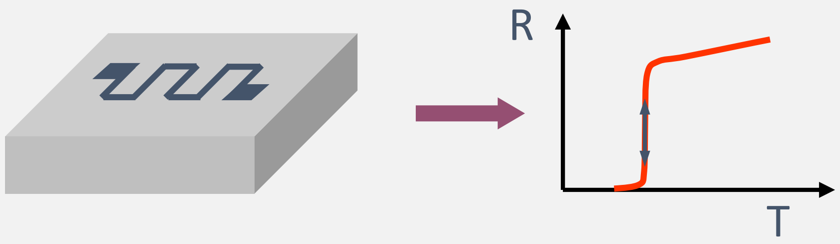

Magnetization of paramagnetic material, MMC

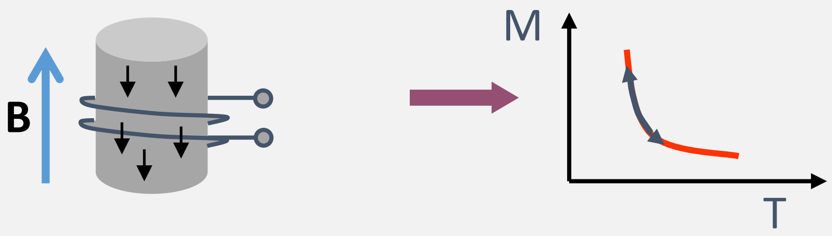

Metallic Magnetic Calorimeters

A.Fleischmann, C. Enss and G. M. Seidel,
Topics in Applied Physics **99** (2005) 63

A.Fleischmann et al.,
AIP Conf. Proc. **1185** (2009) 571

Paramagnetic temperature sensor

Dilute alloy Au:Er or Ag:Er   (Er concentration: a few hundred ppm)

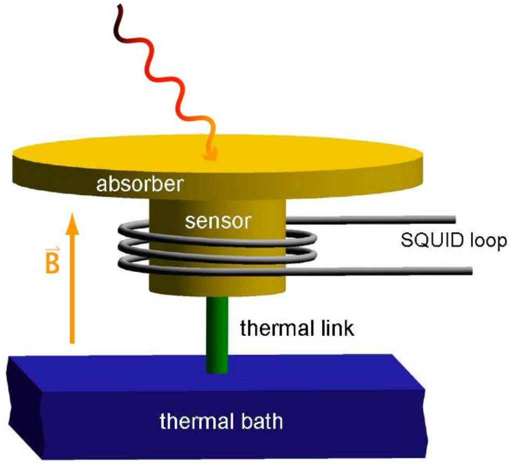

$$\Delta T \cong \frac{E}{C_{\mathrm{tot}}}$$

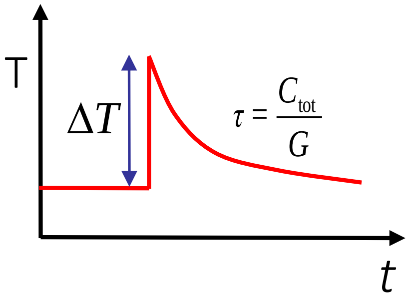

Metallic Magnetic Calorimeters

A.Fleischmann, C. Enss and G. M. Seidel, Topics in Applied Physics **99** (2005) 63

A.Fleischmann et al., *AIP Conf. Proc.* **1185** (2009) 571

Paramagnetic temperature sensor

Dilute alloy Au:Er or Ag:Er (Er concentration: a few hundred ppm)

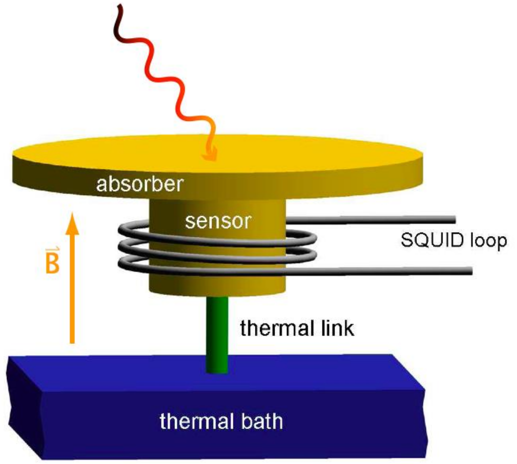

$$\Delta T \cong \frac{E}{C_{\mathrm{tot}}} \xrightarrow{\text{MMC}} \Delta\Phi_S \propto \frac{\partial M}{\partial T}\Delta T \rightarrow \Delta\Phi_S \propto \frac{\partial M}{\partial T}\frac{E}{C_{\mathrm{tot}}}$$

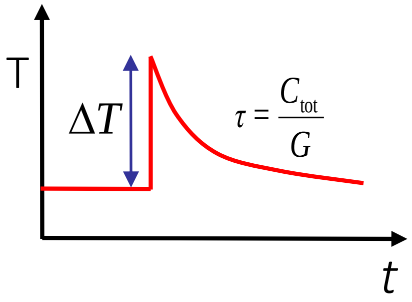

Metallic Magnetic Calorimeters

A.Fleischmann, C. Enss and G. M. Seidel,
Topics in Applied Physics **99** (2005) 63

A.Fleischmann et al.,
AIP Conf. Proc. **1185** (2009) 571

Paramagnetic temperature sensor

Dilute alloy Au:Er or Ag:Er (Er concentration: a few hundred ppm)

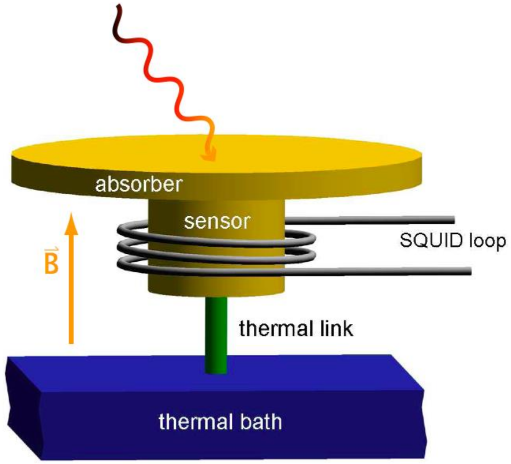

$$\Delta T \cong \frac{E}{C_{tot}} \xrightarrow{\text{MMC}} \Delta\Phi_S \propto \frac{\partial M}{\partial T}\Delta T \rightarrow \Delta\Phi_S \propto \frac{\partial M}{\partial T}\frac{E}{C_{tot}}$$

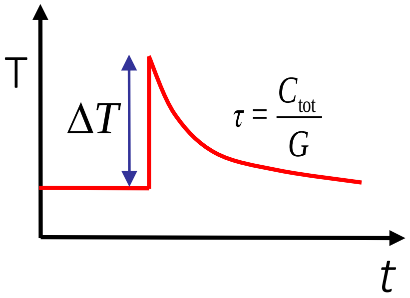

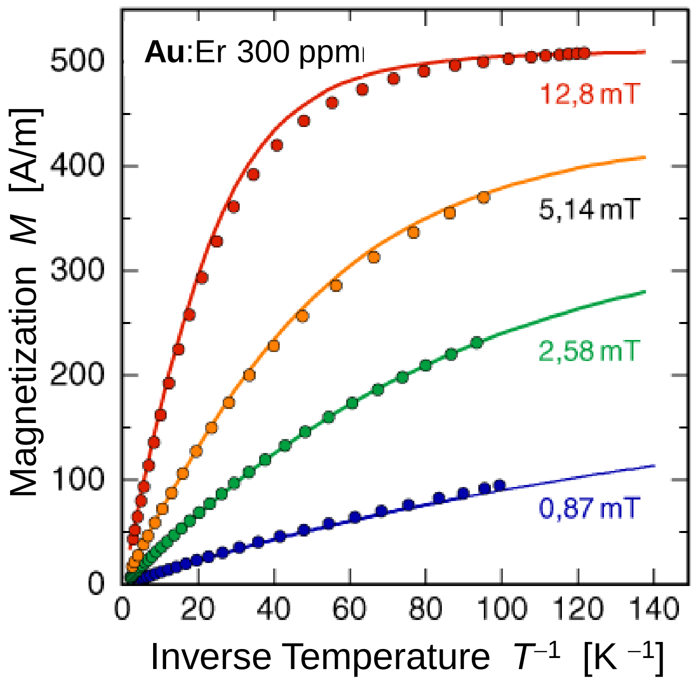

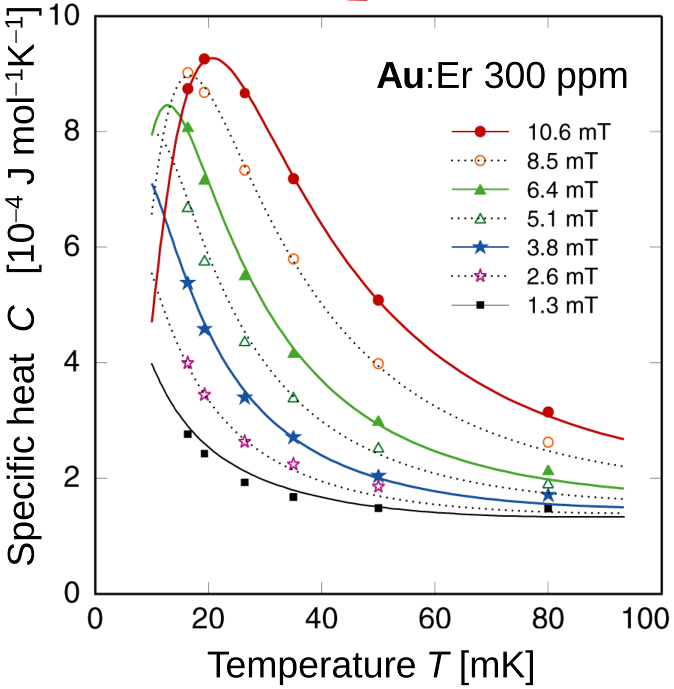

Very good agreement between data and theoretical expectation for interacting spin system

Performance

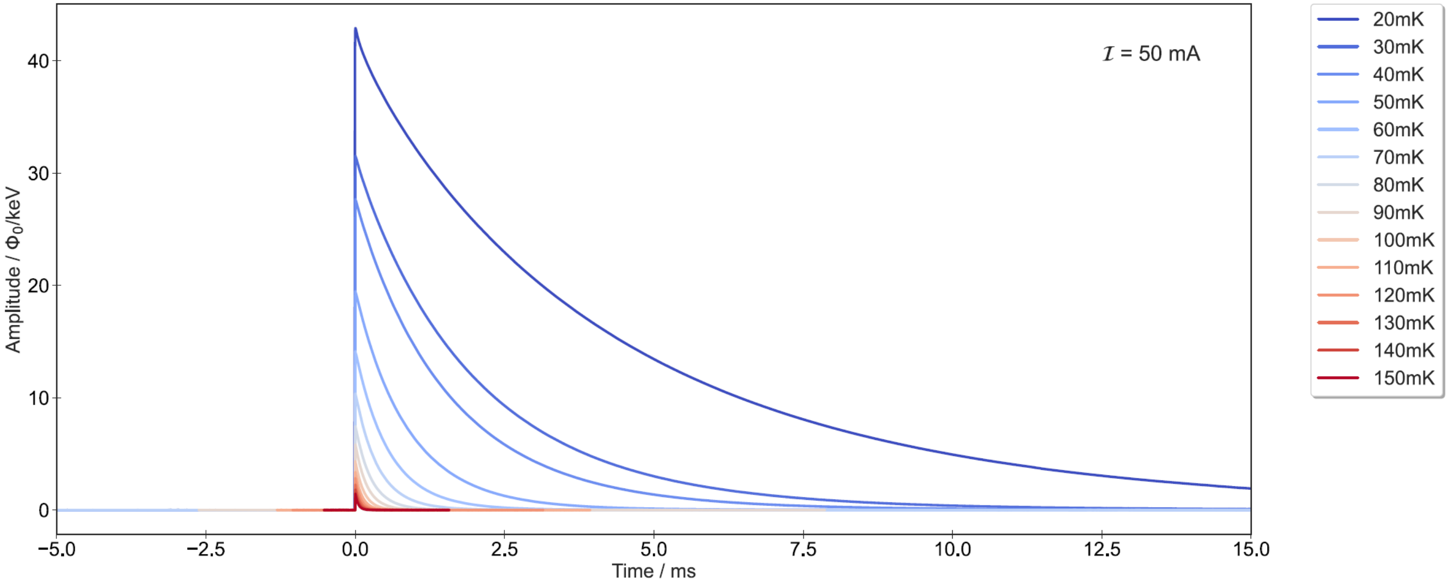

Operation over a large temperature range
→ operation of large arrays

Large dynamic range
→ no saturation of the signal

Design defined decay constant
→ thermal link optimized for detector heat capacity at operating temperature

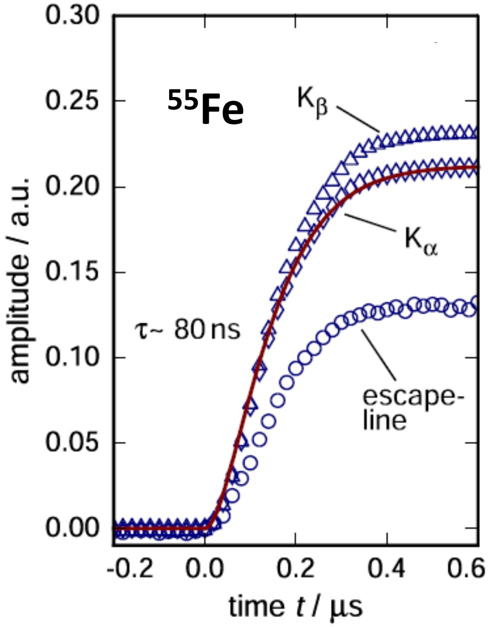

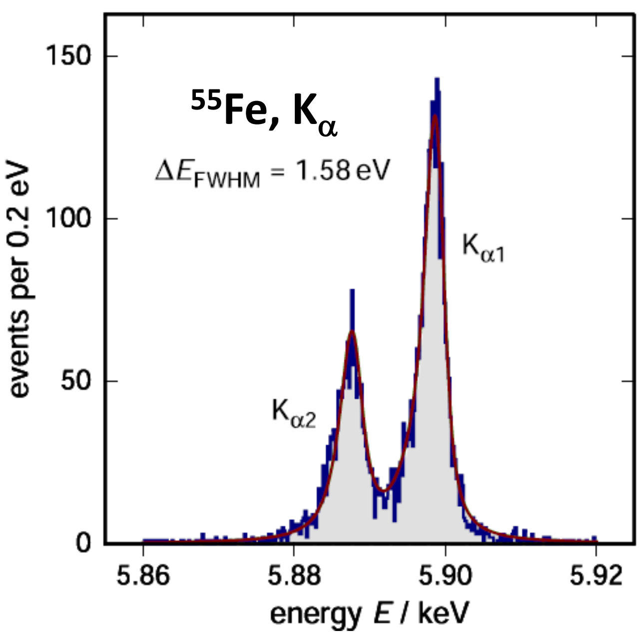

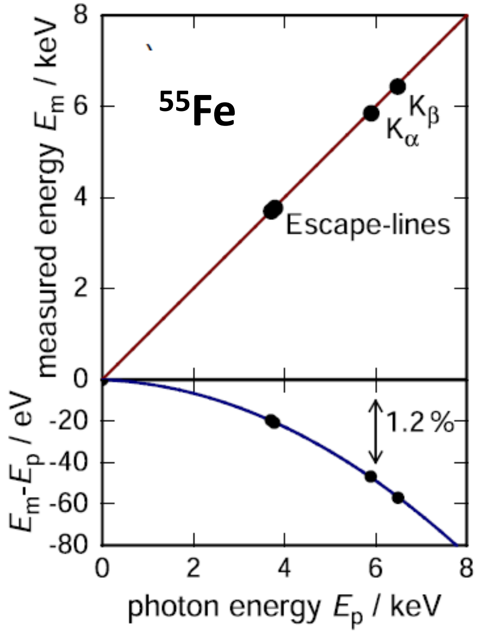

Fast risetime
→ Reduction un-resolved pile-up

Extremely good energy resolution
→ identification of small structures

Excellent linearity
→ precise definition of the energy scale

Detector geometries

- planar paramagnetic sensor
- superconducting coil
- transformed coupled to a dc SQUID

Well established:
- superconducting meander shaped pickup loop
- planar sensor on top of meander-shaped coil
- gradiometric design

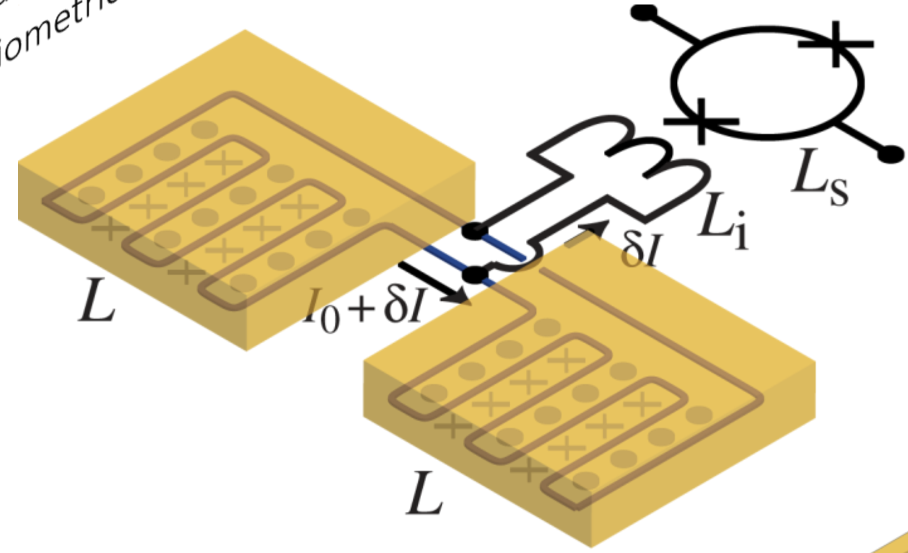

Sandwich geometry:
- planar sensor sandwiched between stripline
- best magnetic flux coupling

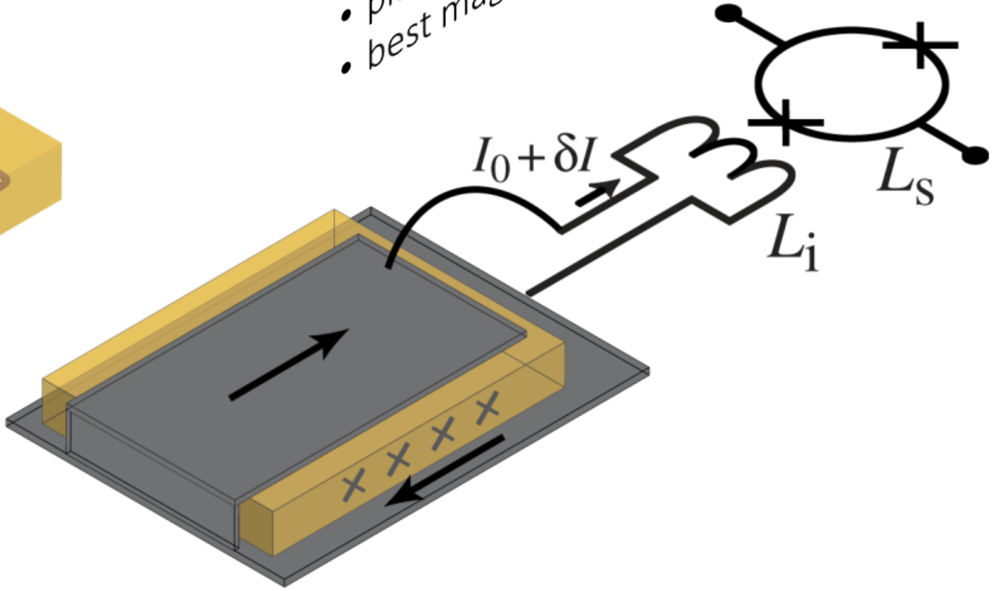

Persistent current

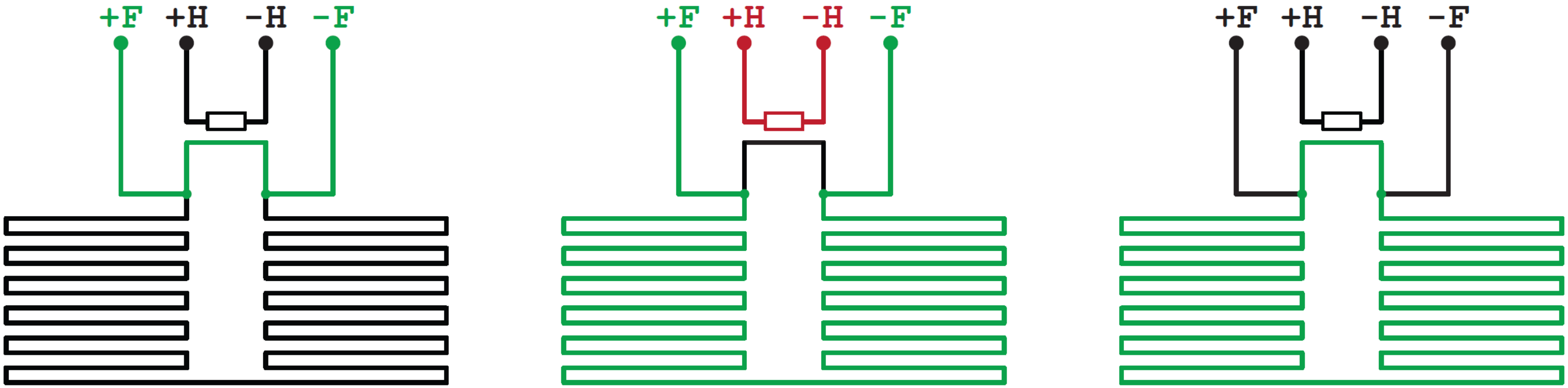

Reliable injection of a persistent current in the superconducting coil:

Achievable critical current density: ~ 10 MA/cm^2

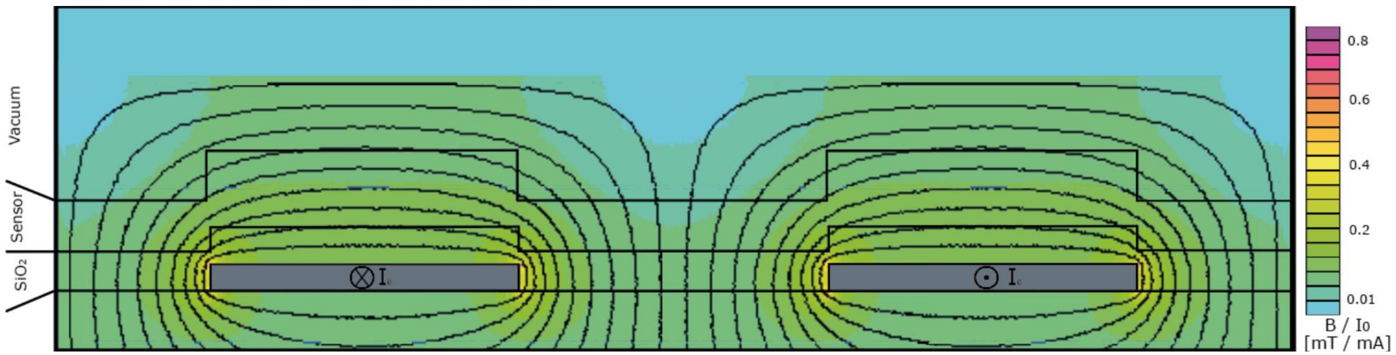

MMC readout

Two-stage dc-SQUID readout with flux-locked loop

low noise

small power dissipation on detector SQUID chip (voltage bias 1st stage)

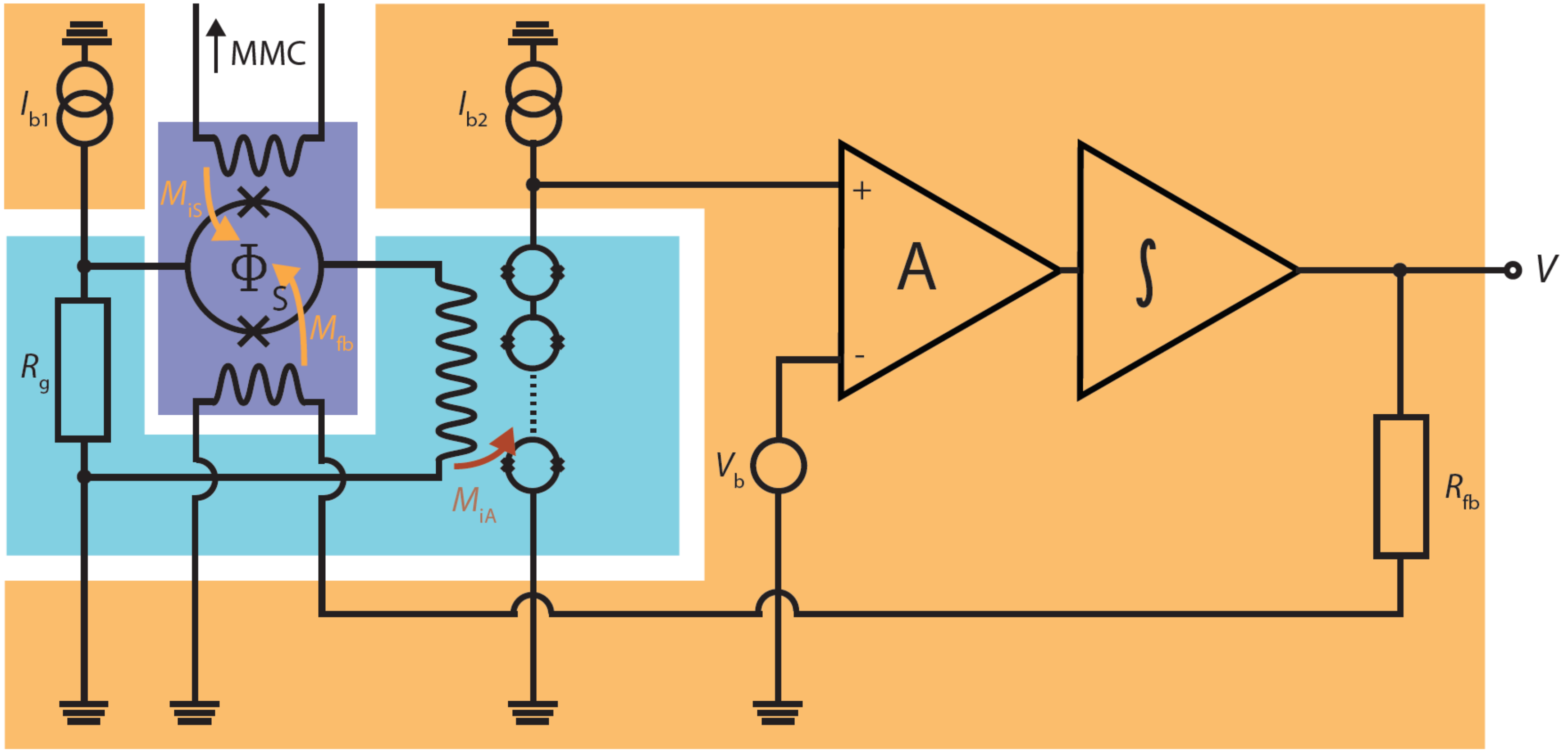

1st stage 2nd stage Room temperature electronics

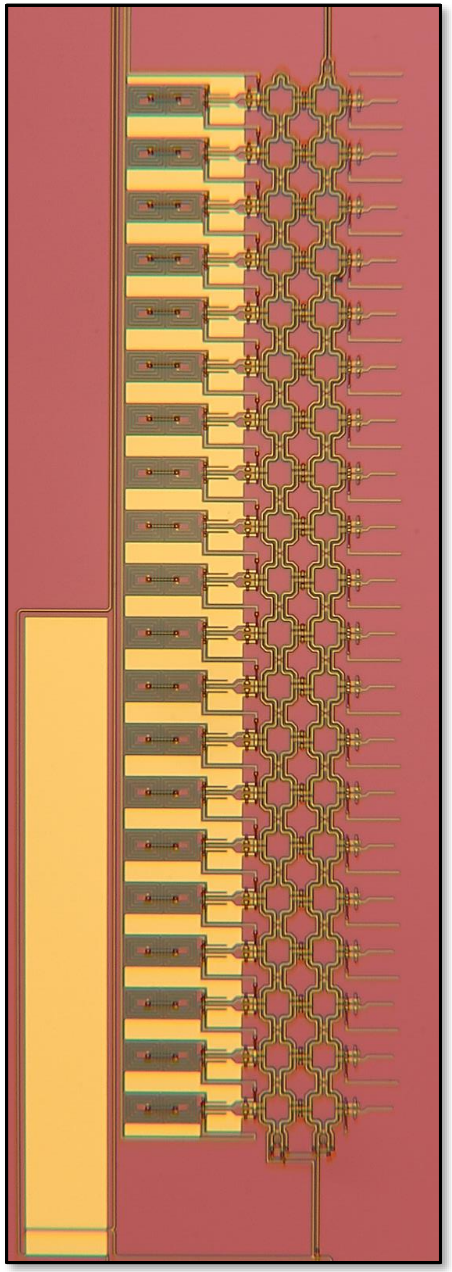

In house produced SQUID array

MMC readout

Detector module

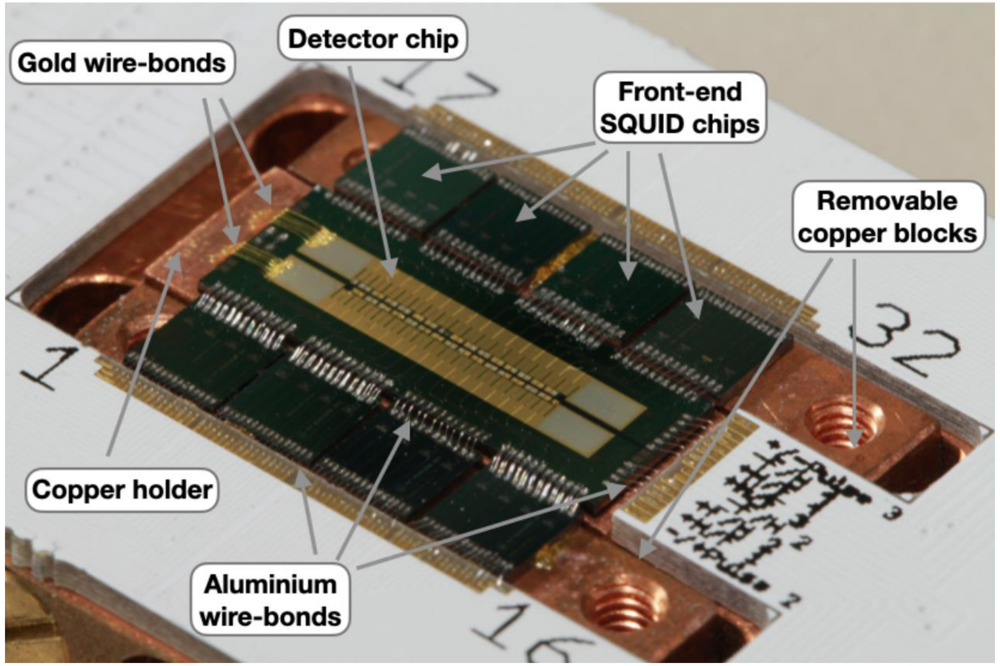

Amplifier module

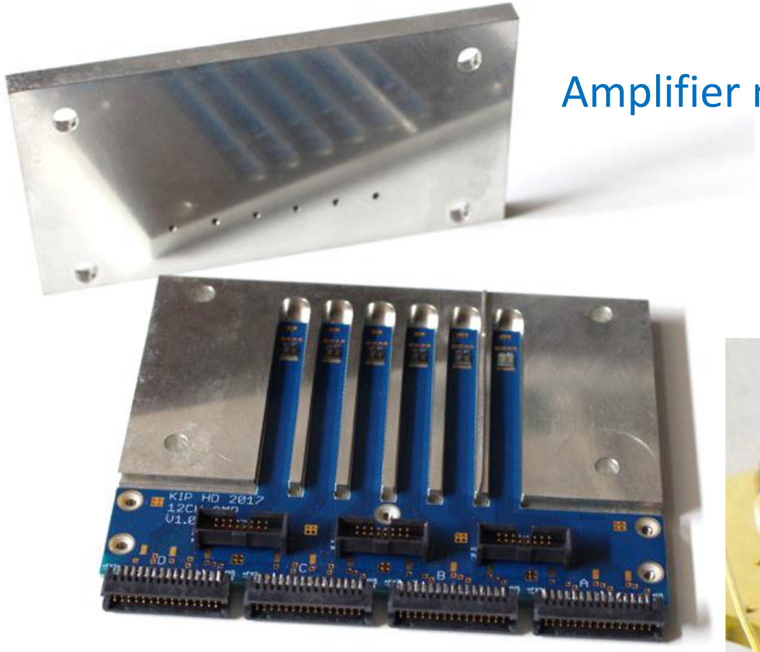

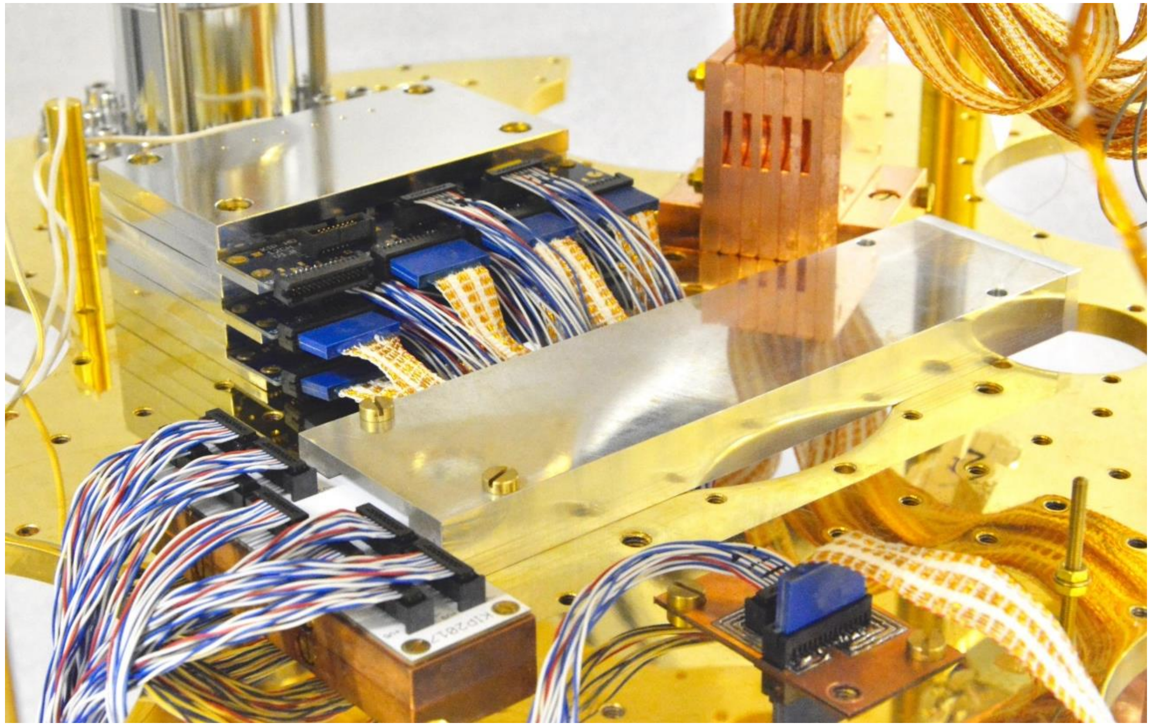

Detector and amplifier module mounted on the mixing chamber plate

F. Mantegazzini et al., *JINST* **16** (2021) P08003, [arXiv:2102.11100](https://arxiv.org/abs/2102.11100) [physics.ins-det]

MMC readout

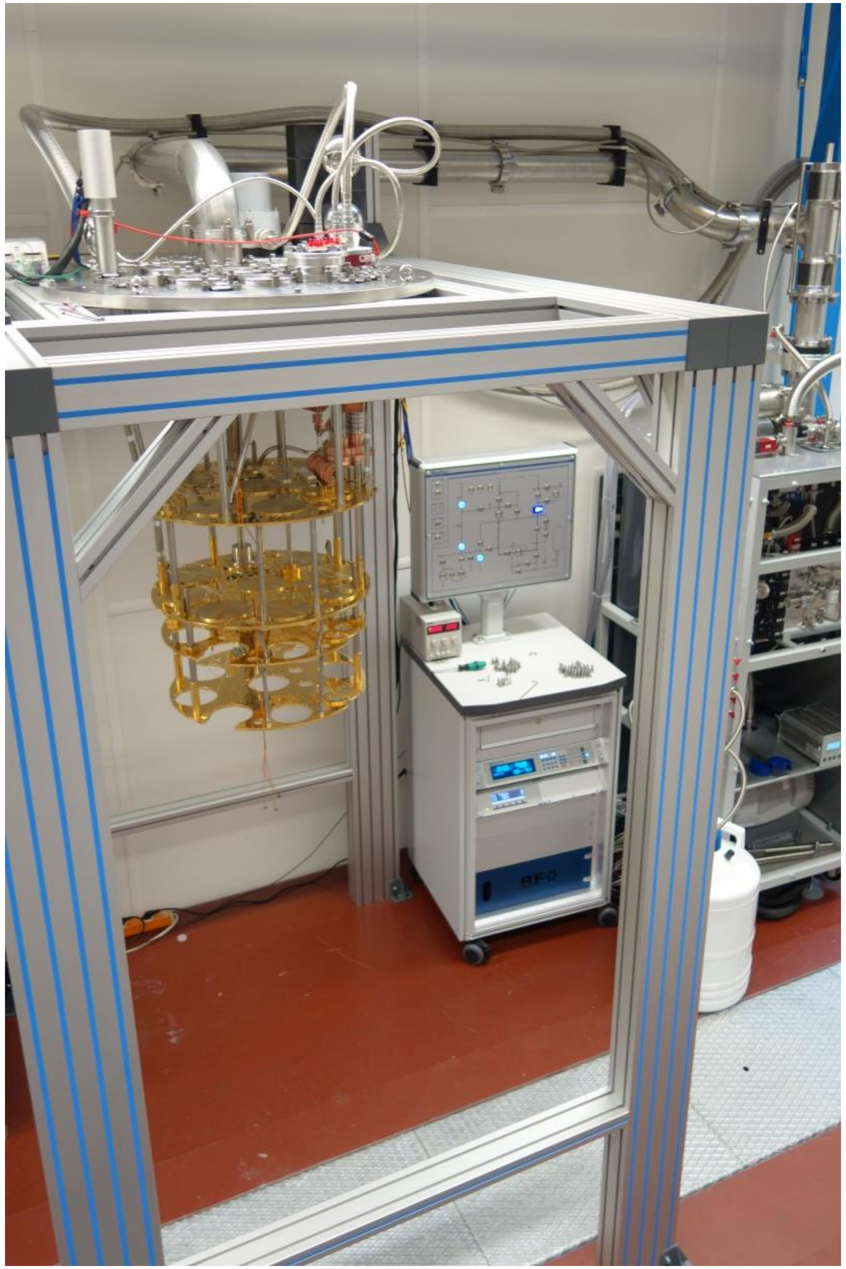

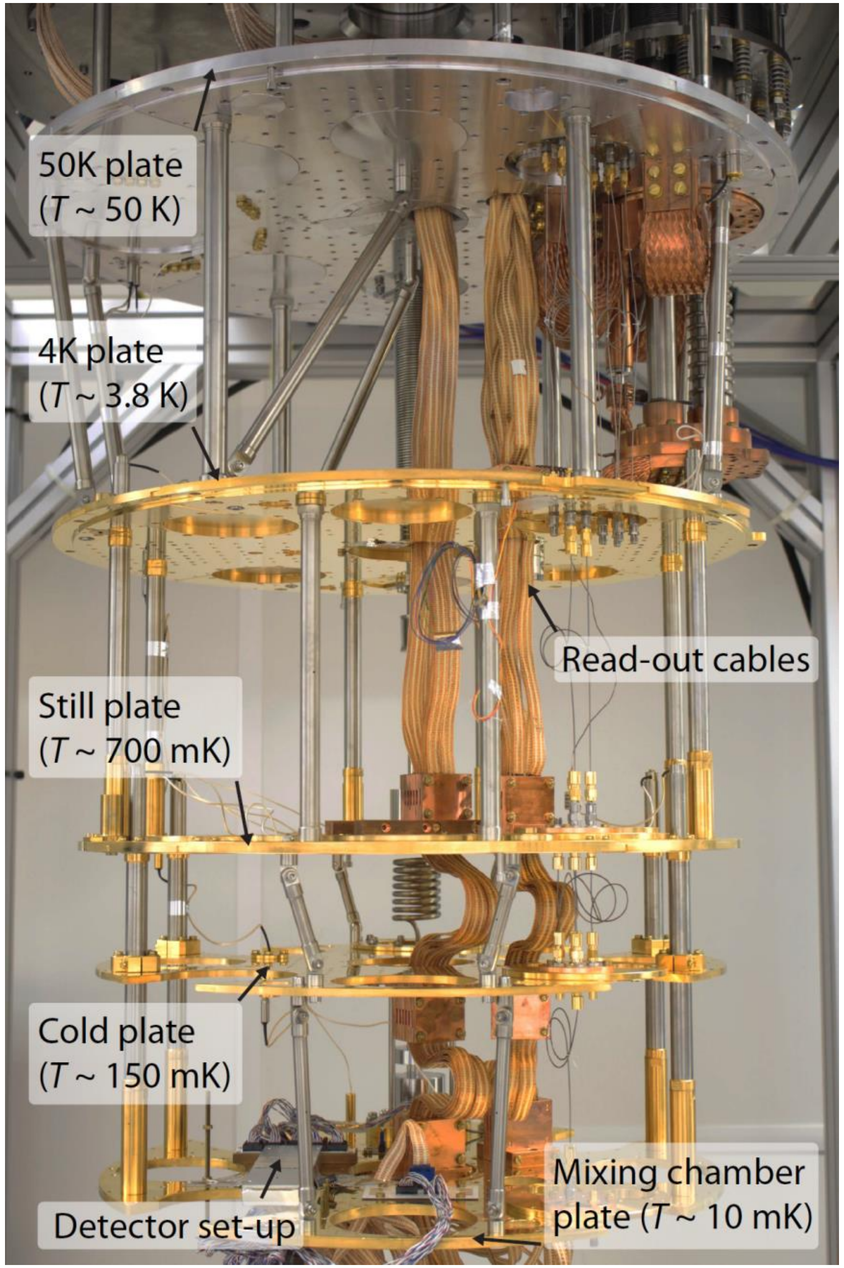
50K plate
(T ~ 50 K)
4K plate
(T ~ 3.8 K)
Read-out cables
Still plate
(T ~ 700 mK)
Cold plate
(T ~ 150 mK)
Mixing chamber
plate (T ~ 10 mK)
Detector set-up

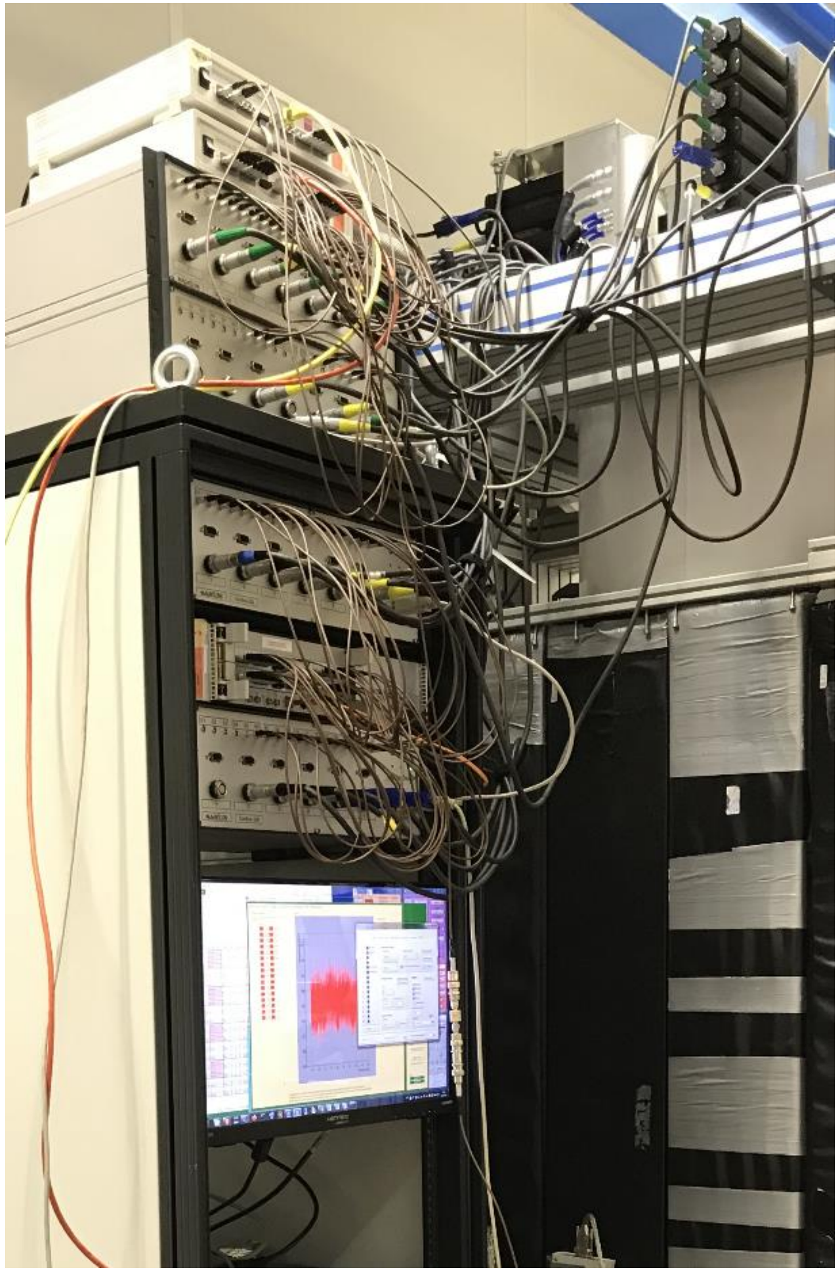

MMC fabrication

40 m^2 Cleanroom class 100
at Kirchhoff Institute for Physics

Wet bench
Chemistry bench
Maskless aligner
UHV sputtering system
Dry etching system

- Flexibility in design and fabrication
- Reliable processes for thin films
- Production of MMC array and superconducting electronics

MMC fabrication

ECHo-100k wafer

Fabrication steps				
#	Layer	Material	Thickness	Deposition technique
1	Pick-up coils, SQUID lines (layer 1)	Nb	250 nm	Sputtering + etching
2	Isolation	Nb_2O_5	-	Anodisation
3	Isolation	SiO_2	175 nm	Sputtering + lift-off
4	Isolation	SiO_2	175 nm	Sputtering + lift-off
5	Heaters	AuPd	150 nm	Sputtering + lift-off
6	SQUID lines (layer 2)	Nb	600 nm	Sputtering + lift-off
7	Sensor	AgEr	480 nm	Sputtering + lift-off
8	Thermalisation	Au	300 nm	Sputtering + lift-off
9	Stems	Au	100 nm	Sputtering
10	Absorber - 1st layer	Au	3 µm	Electroplating + lift-off
11	^{163}Ho host material	Ag	100 nm	Sputtering
12	^{163}Ho implantation	^{163}Ho	-	Ion-implantation
13	^{163}Ho host material	Ag	100 nm	Sputtering + lift-off
14	Absorber - 2nd layer	Au	3 µm	Sputtering + lift-off

F. Mantegazzini, PhD Dissertation, Heidelberg University, 2021

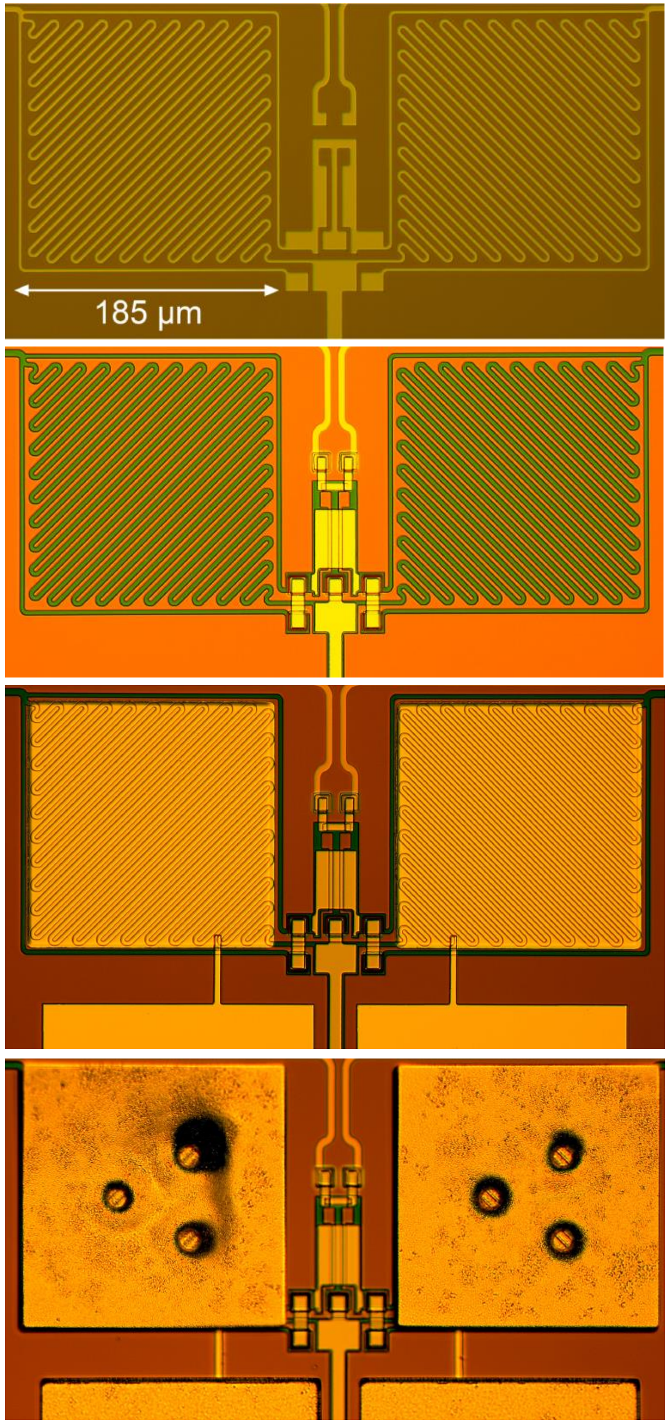

Applications and Performance

Microcalorimeter arrays for X-rays spectroscopy - maXs

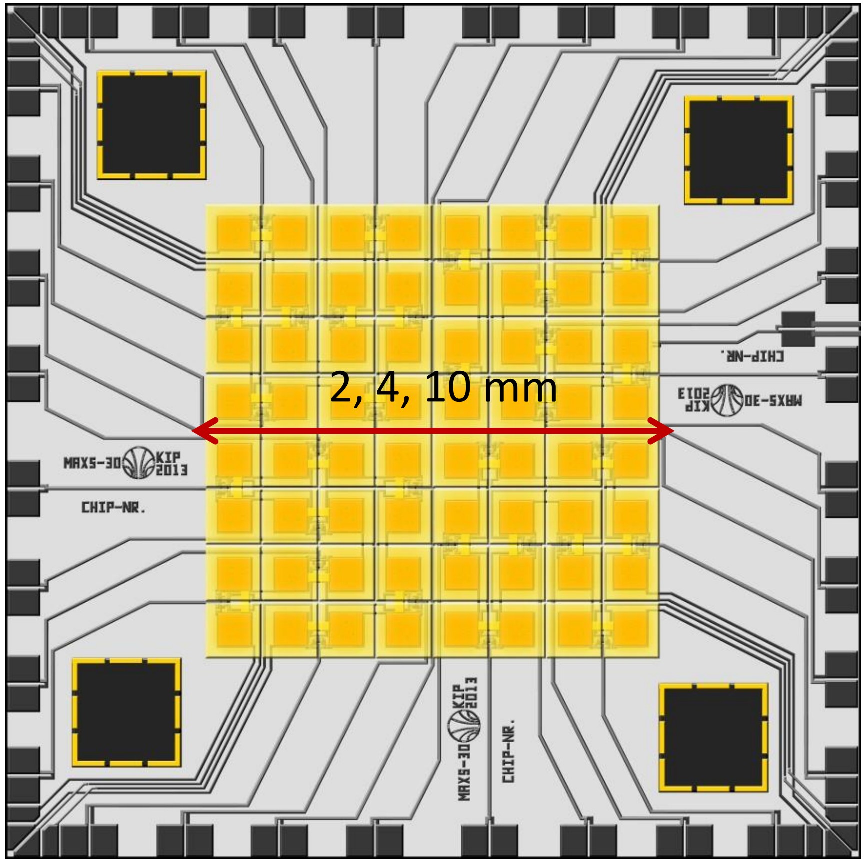

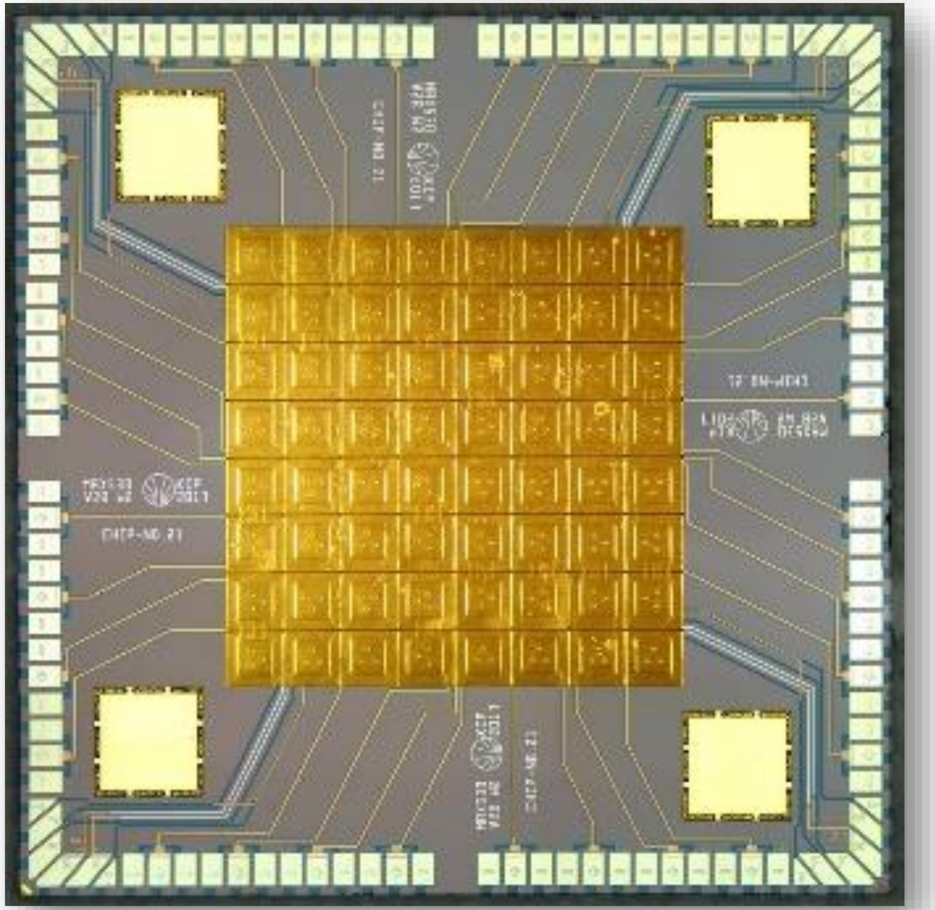

8 mm

maXs-20/30/100:

- 8×8 pixels for photons up to 20/30/100 keV
- with ΔE_{FWHM} = 2/5/30 eV
- 32 two-stage dc-SQUIDs

maXs-30

Absorber size: 500 × 500 × 30 μm^3

maXs-30 set-up for IAXO

Search for an evidence for solar axions

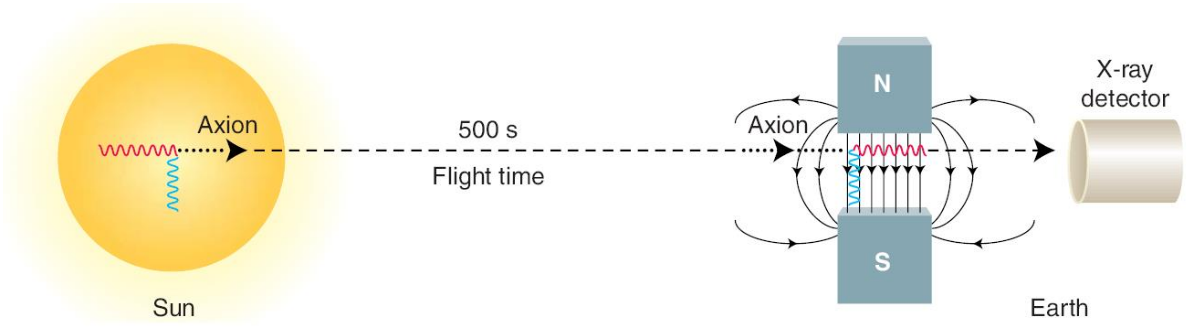

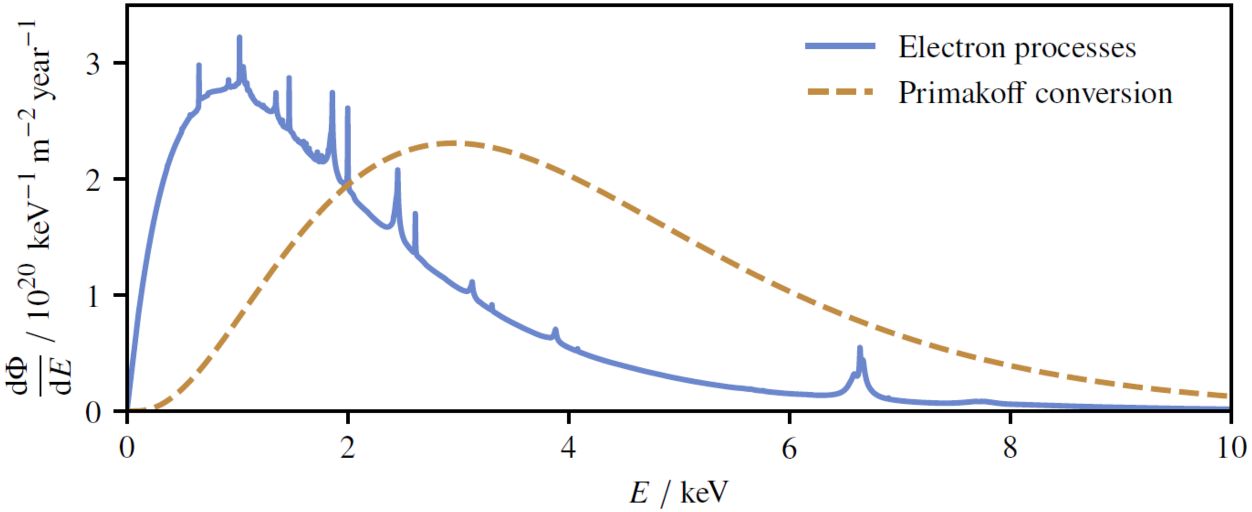

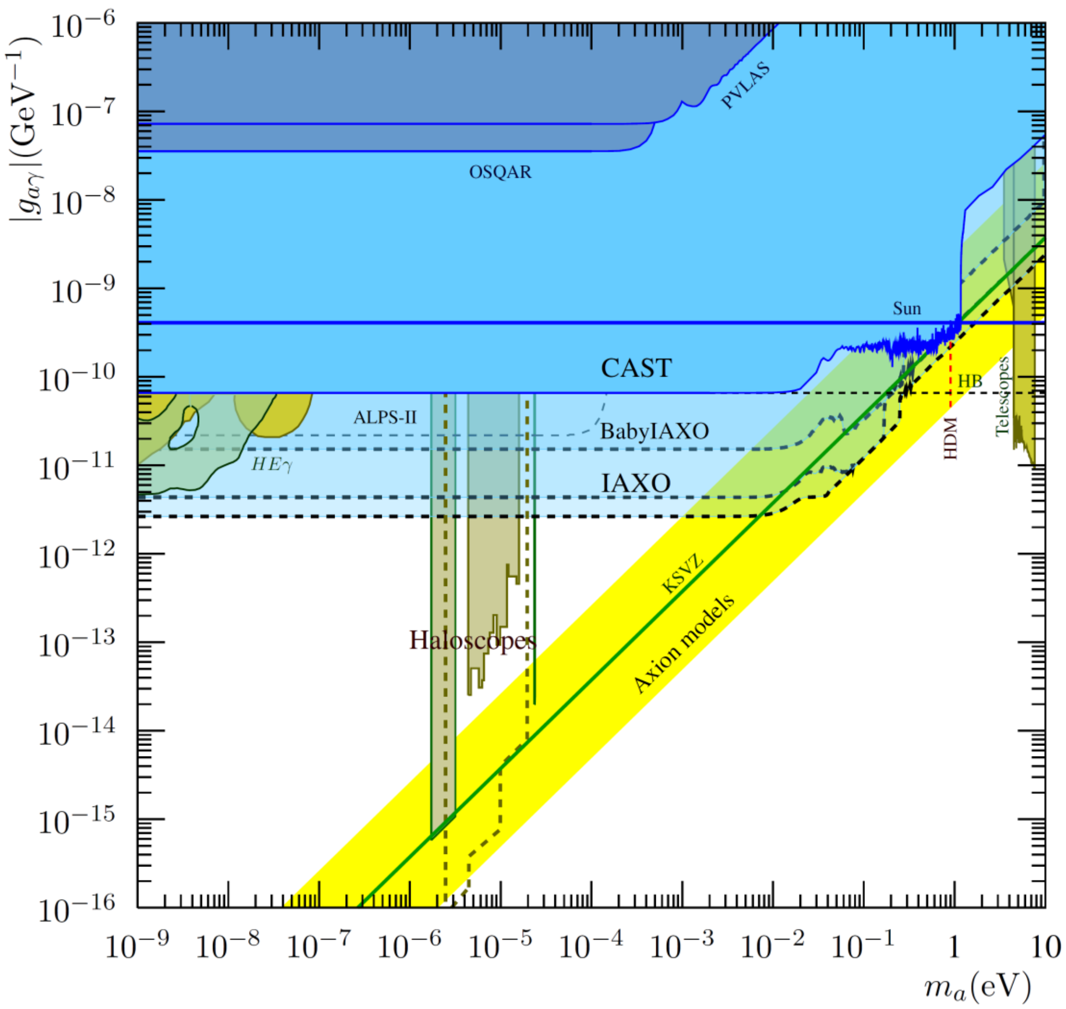

Low background and high energy resolution (low threshold) x-ray detectors

The IAXO Collaboration, *Journal of High Energy Physics* **2021** 137 (2021)

maXs-30 set-up for IAXO

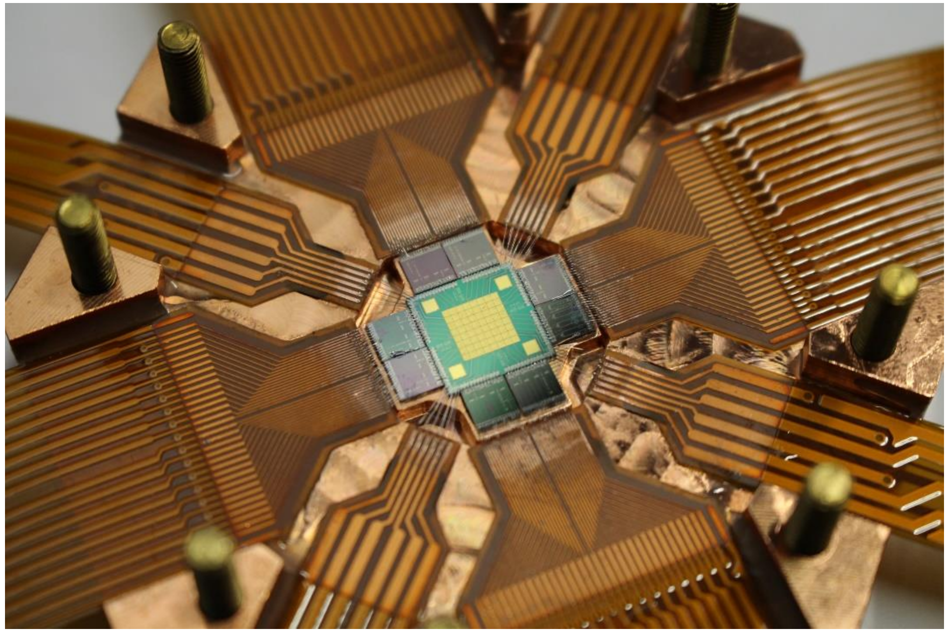

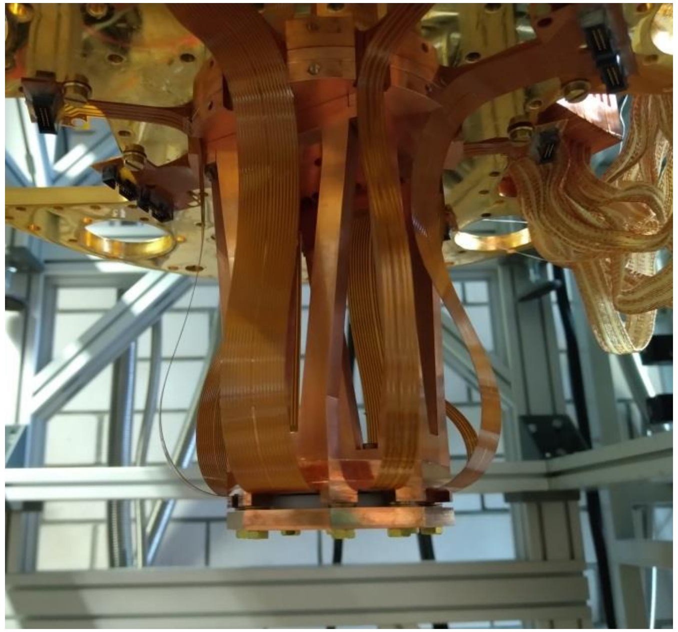

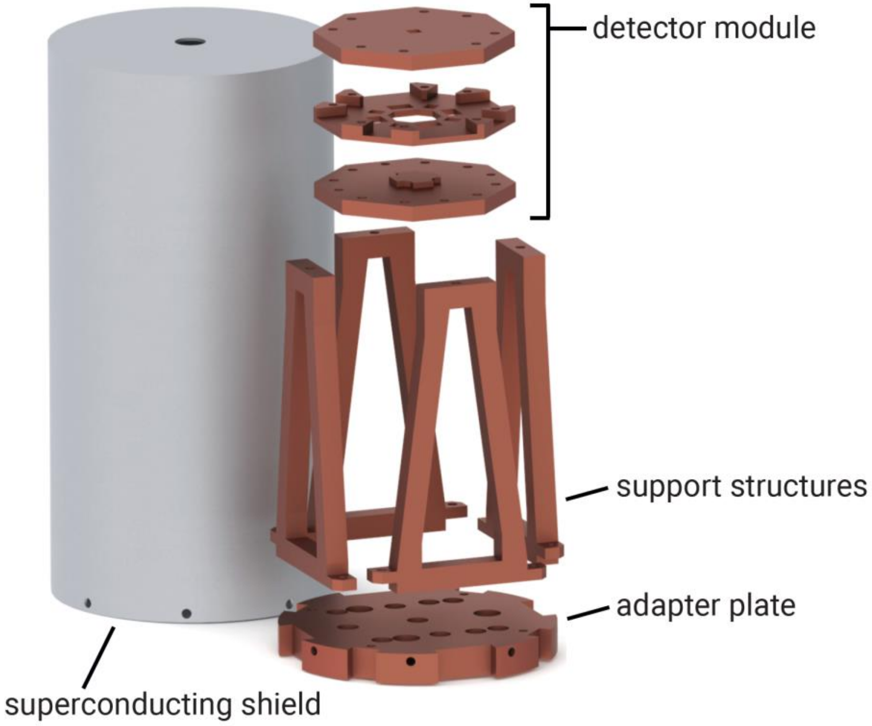

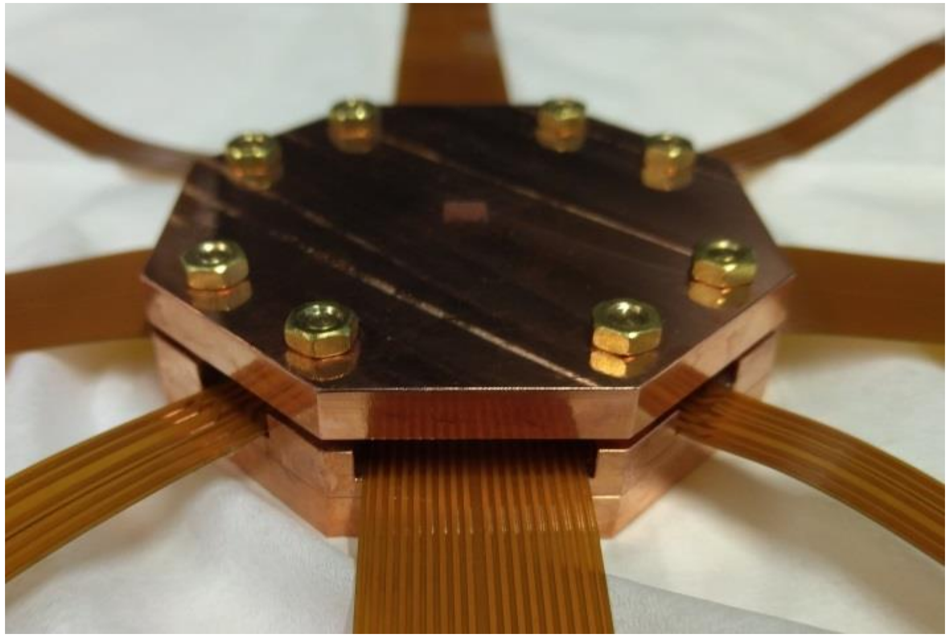

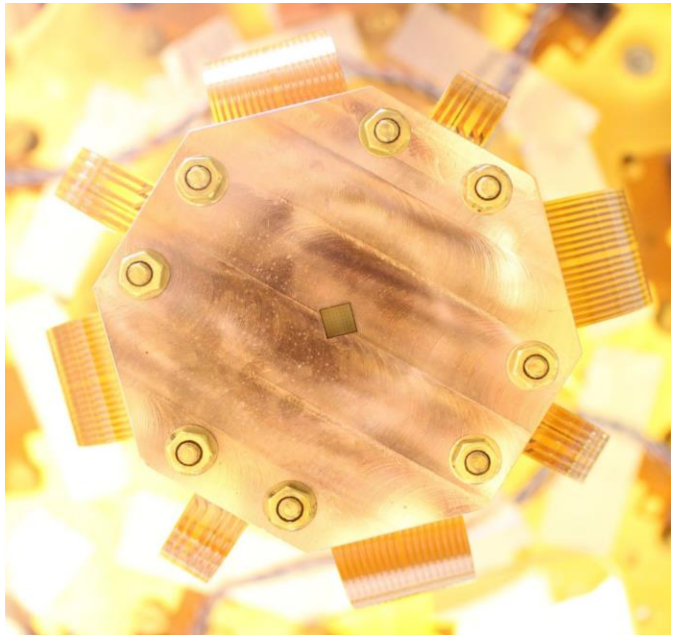

Design suitable for IAXO telescope

High purity materials for background reduction

D. Unger et al., *JINST* **16** (2021) P06006, arXiv:2010.15348 [physics.ins-det]

maXs-30 set-up for IAXO

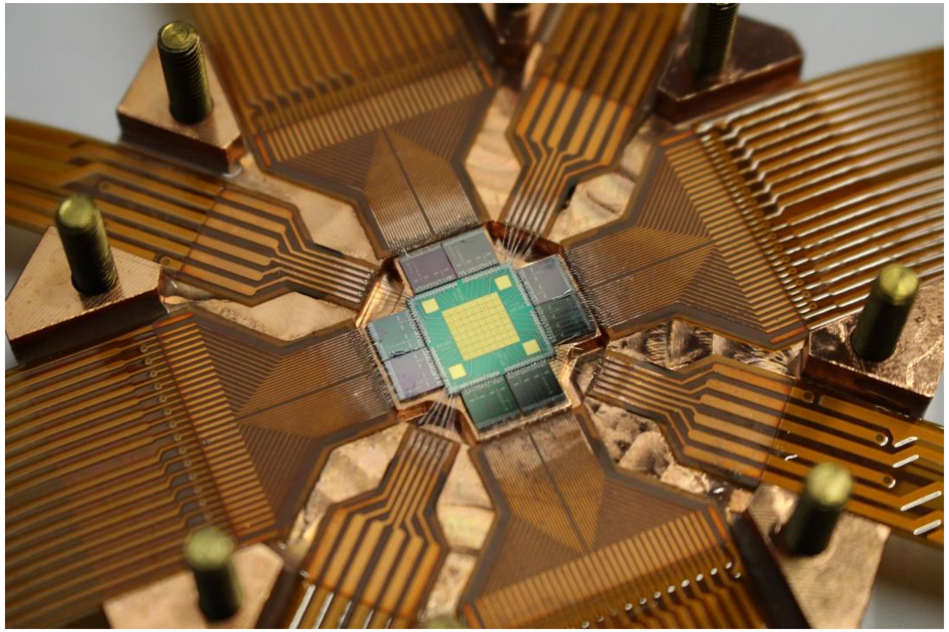

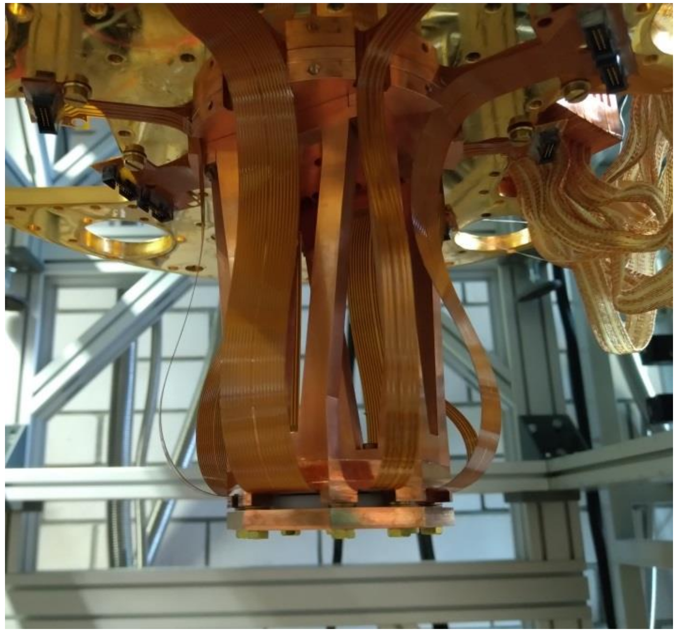

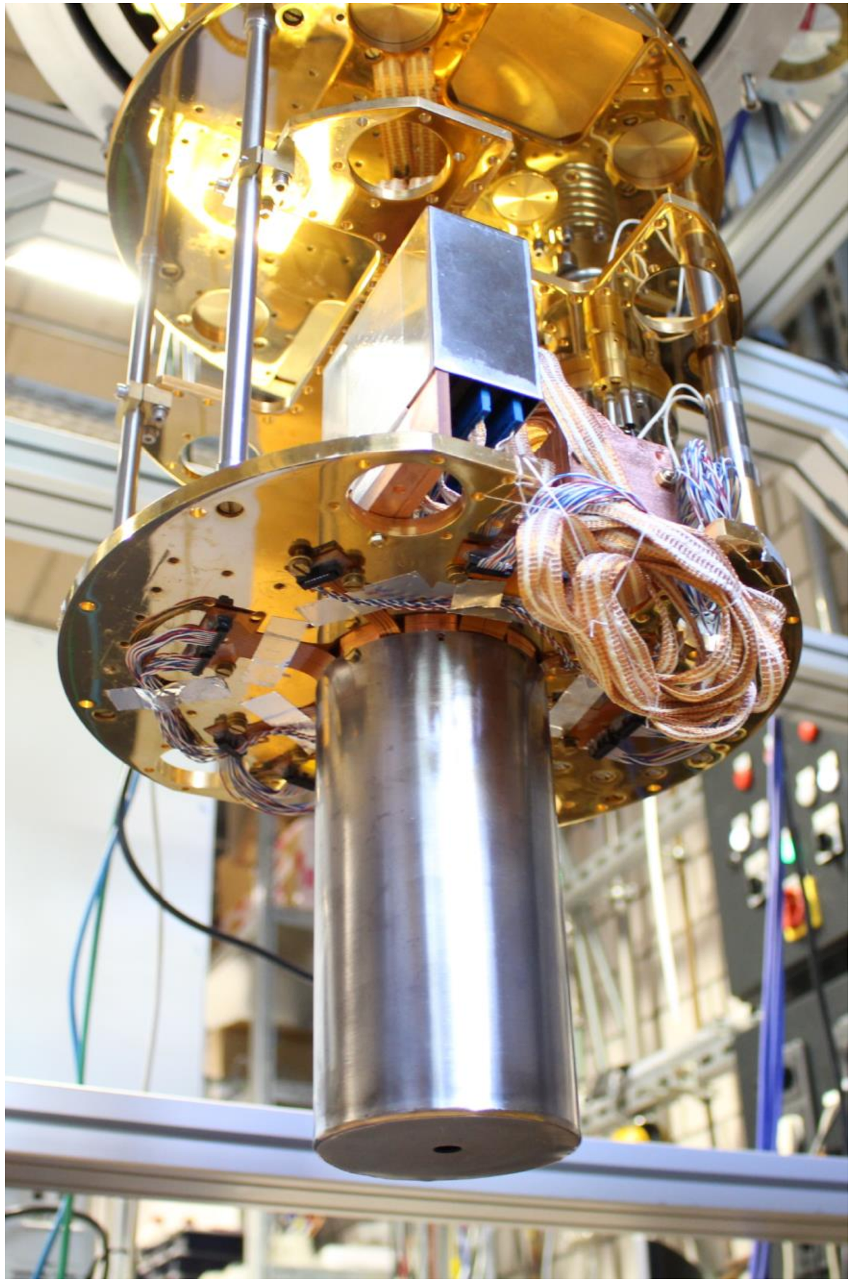

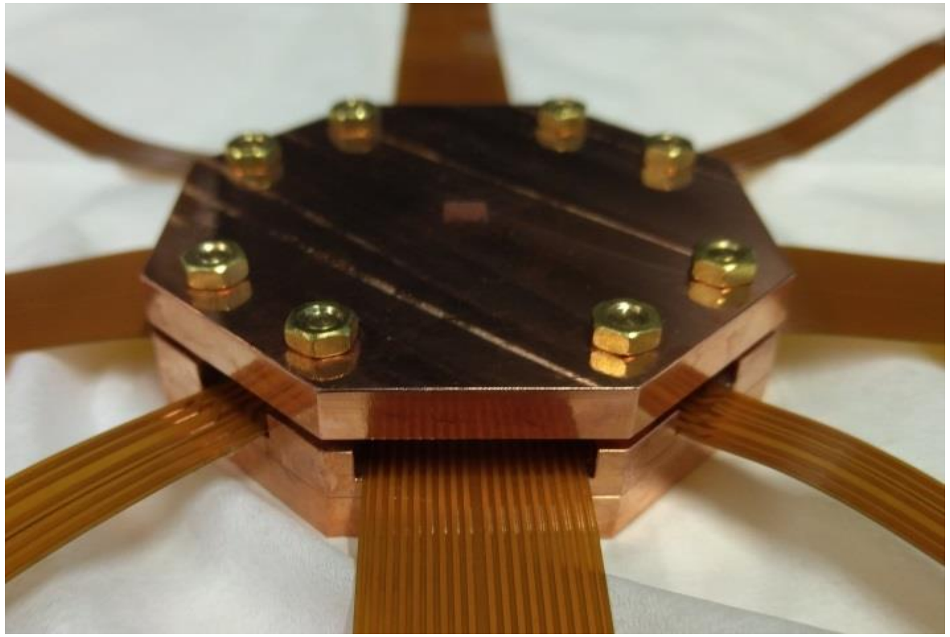

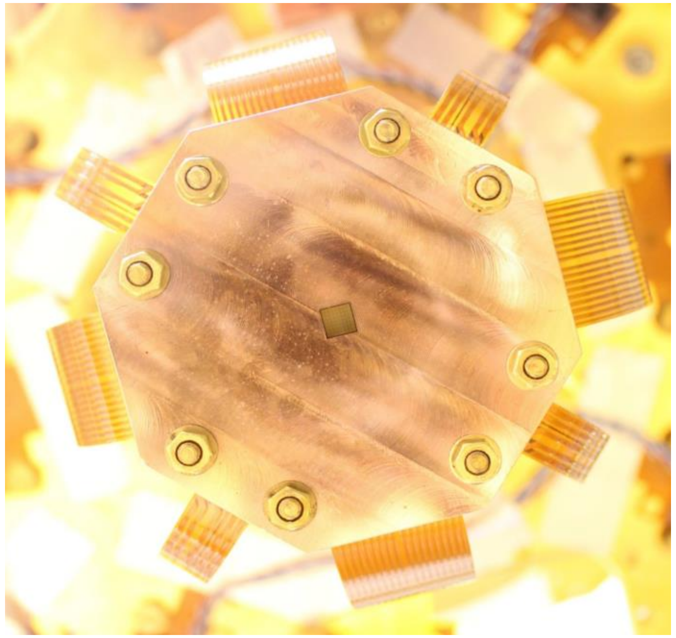

maXs-30 set-up for IAXO

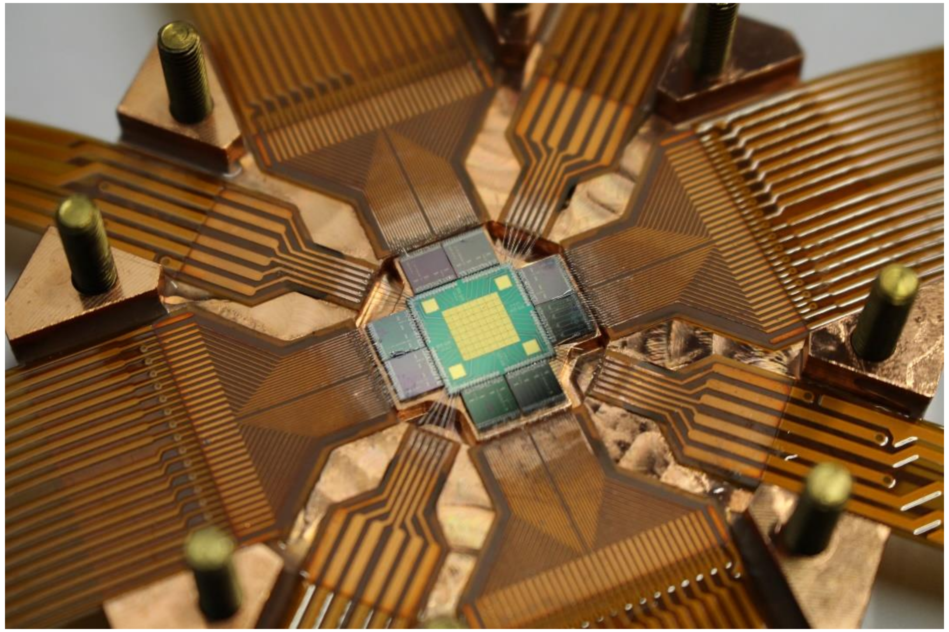

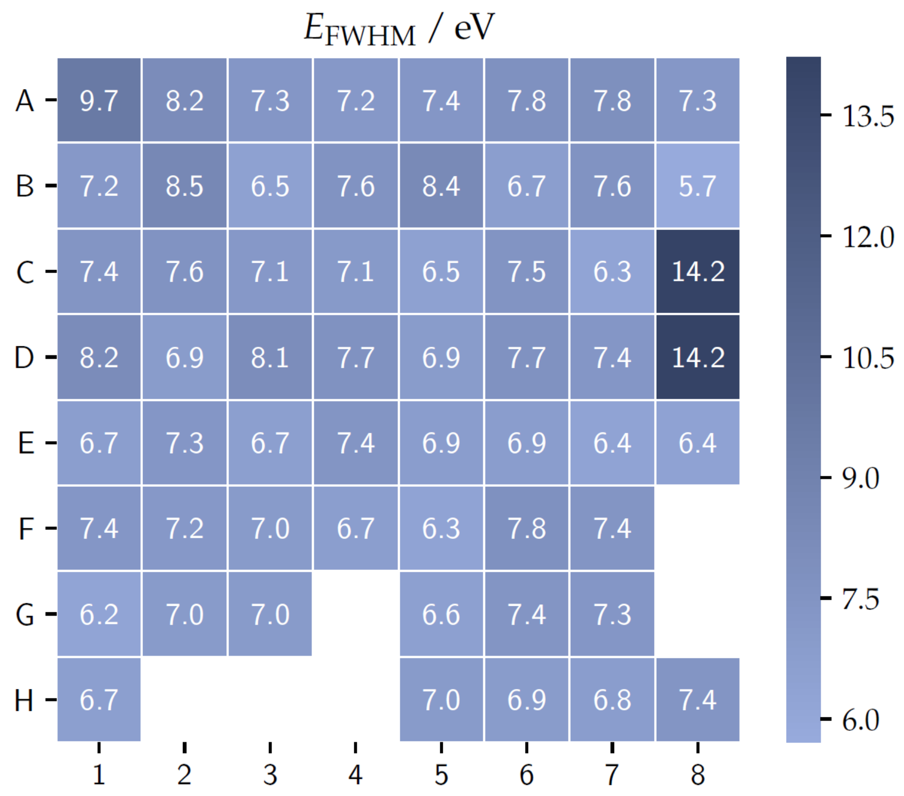

^{55}Fe calibration source
Stopping power @10 keV ~100%

- Homogeneous performance over the array
- Stable operation over 1 month

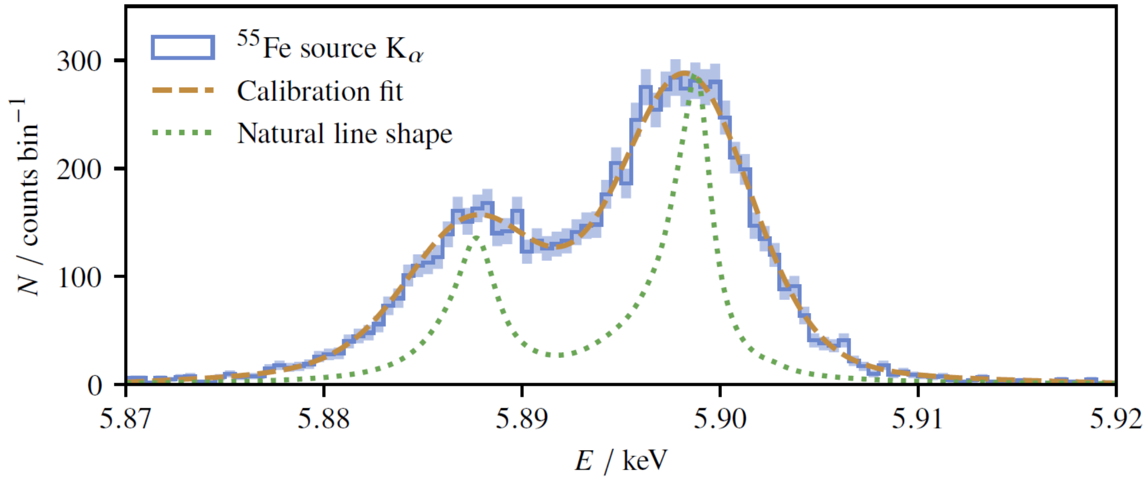

D. Unger et al., *JINST* **16** (2021) P06006,
arXiv:2010.15348 [physics.ins-det]

maXs-30 with ^{241}Am + ^{233}U external sources

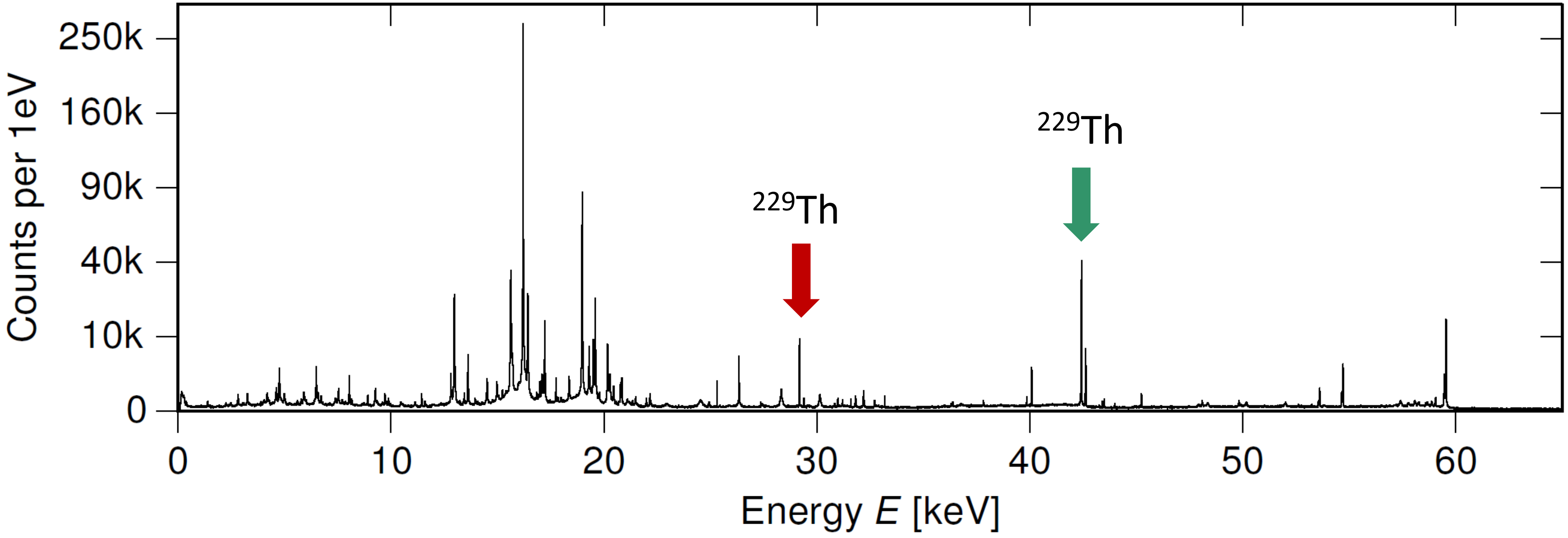

Co-added 20 channels, several weeks

T. Sikorsky et al., *Phys. Rev. Lett.* **125** (2020) 142503

maXs-30 with ^{241}Am + ^{233}U external sources

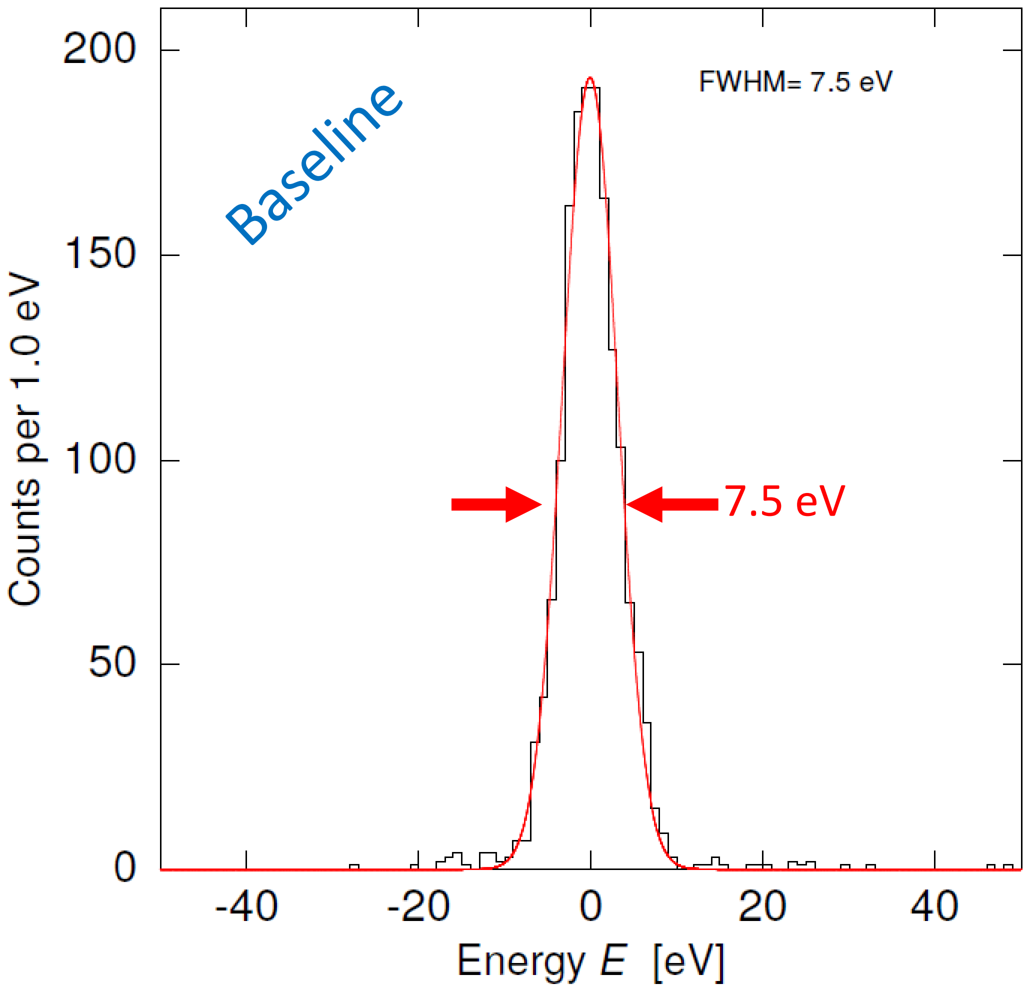

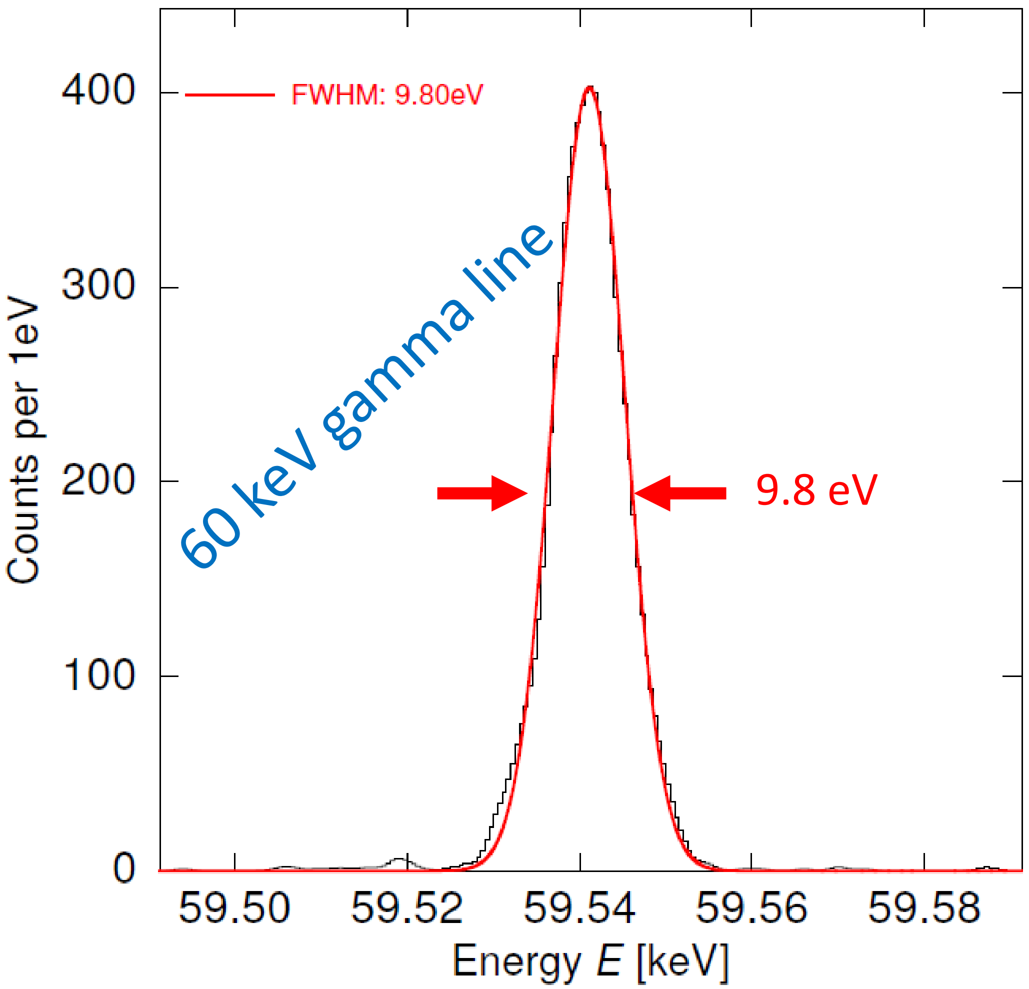

Very close to design value

Energy resolution ΔE_{FWHM} = 9.8 eV @ 59 keV

World record resolving power: 6000

T. Sikorsky et al., *Phys. Rev. Lett.* **125** (2020) 142503

maXs-30 with ^{241}Am + ^{233}U external sources

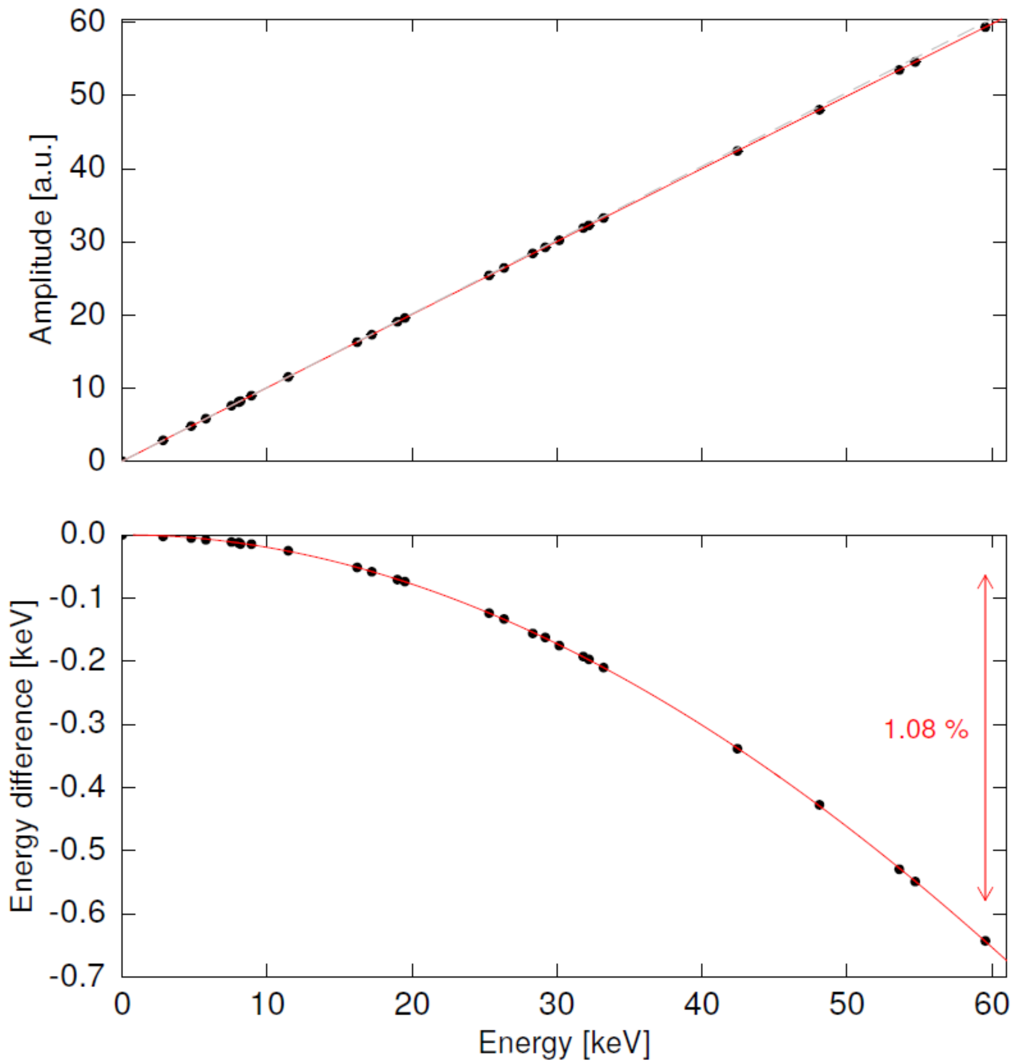

Energy calibration

- Polynomial function 2nd to 4th order
- Stable over long measuring time

non-linearity as expected from thermodynamics!

T. Sikorsky et al., *Phys. Rev. Lett.* **125** (2020) 142503

From maXs-30 to maXs-100

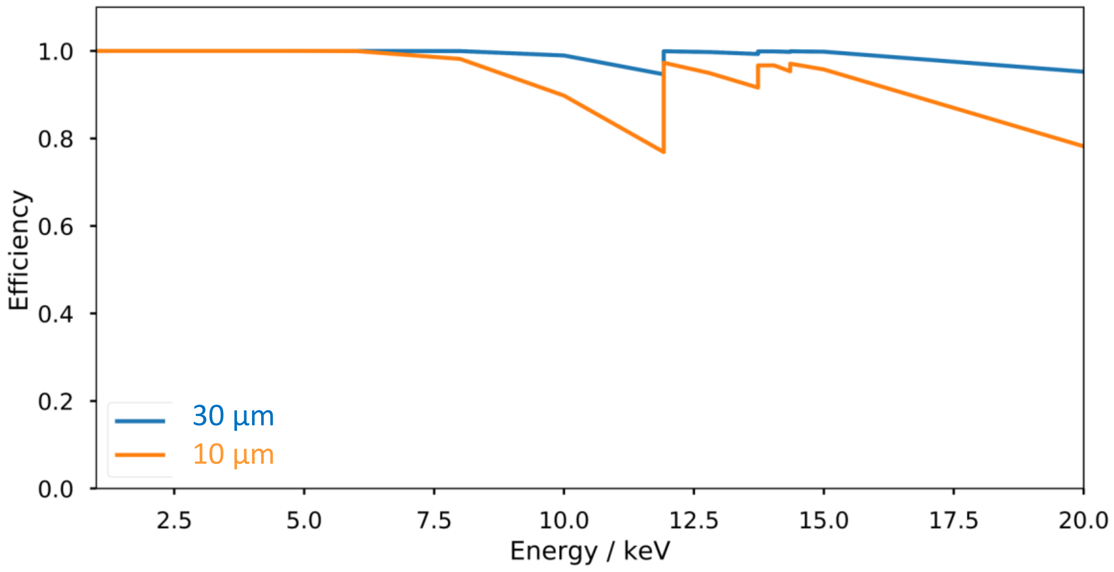

Absorber volume can be adjusted for the particles to be detected

Sensor volume is optimized to match the heat capacity of the absorber at the working temperature

Same design, but scaled up!

maXs-30

8 mm

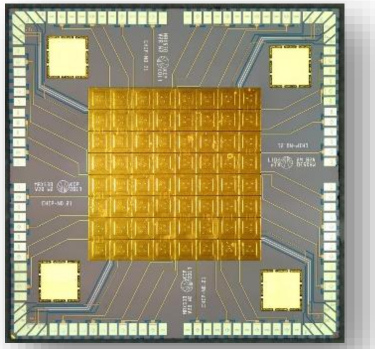

Highly charged ion spectroscopy

maXs-100

15 mm

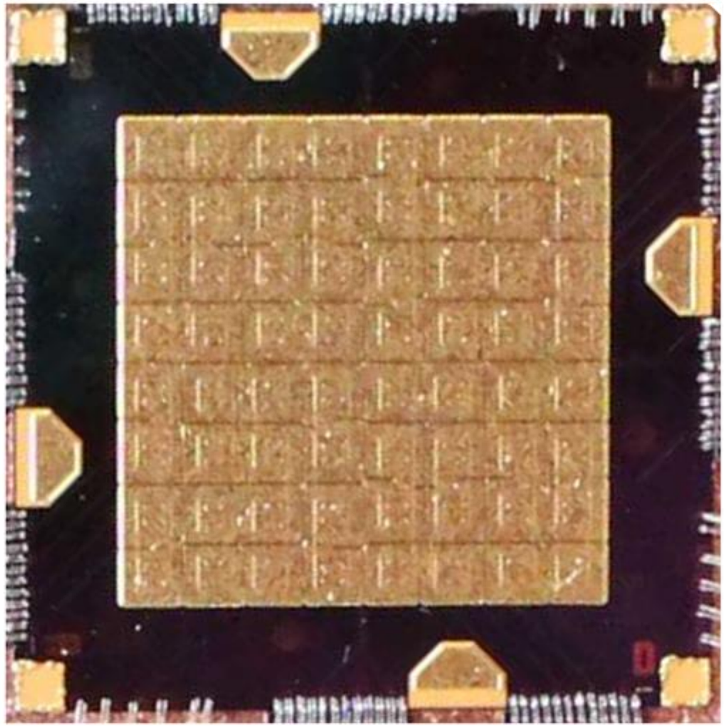

Large area/Lamb shift U^{91+}

32 readout channels for 4000 pixels

32 readout channels for 4000 pixels

1) The Hydra principle

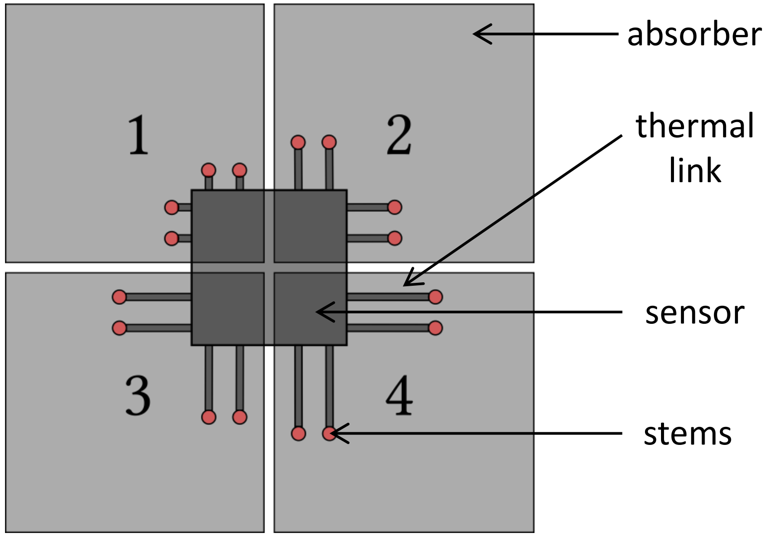

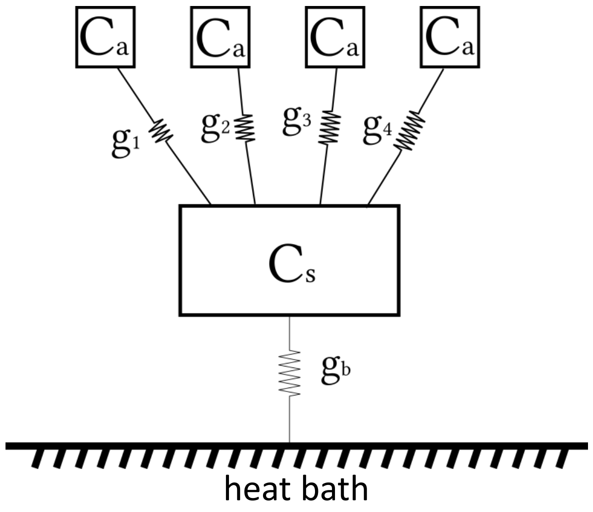

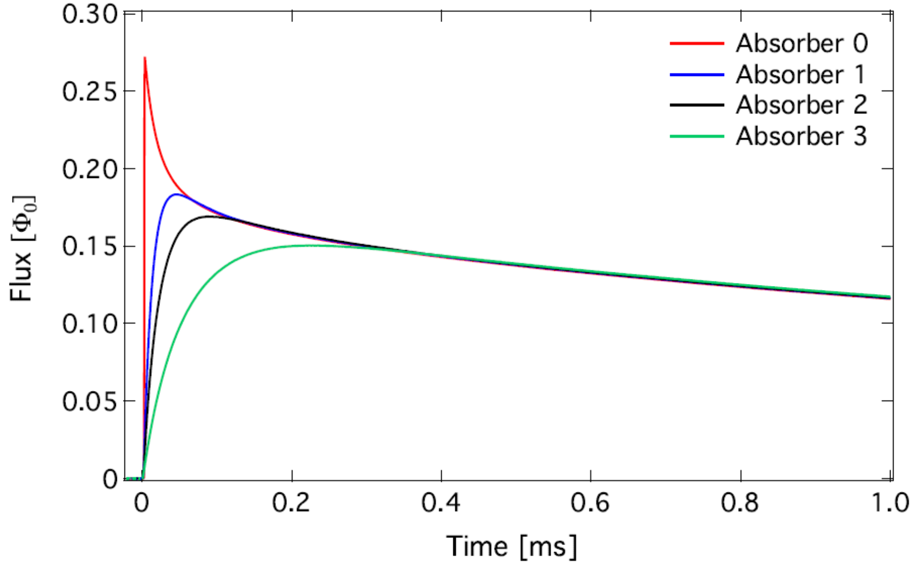

Pixel identification via rise-time of the detector signal

Porst *et al.*, AIP Conf. Proc. **1185** (2009) 599

32 readout channels for 4000 pixels

1) The Hydra principle
2) Segmented sensor

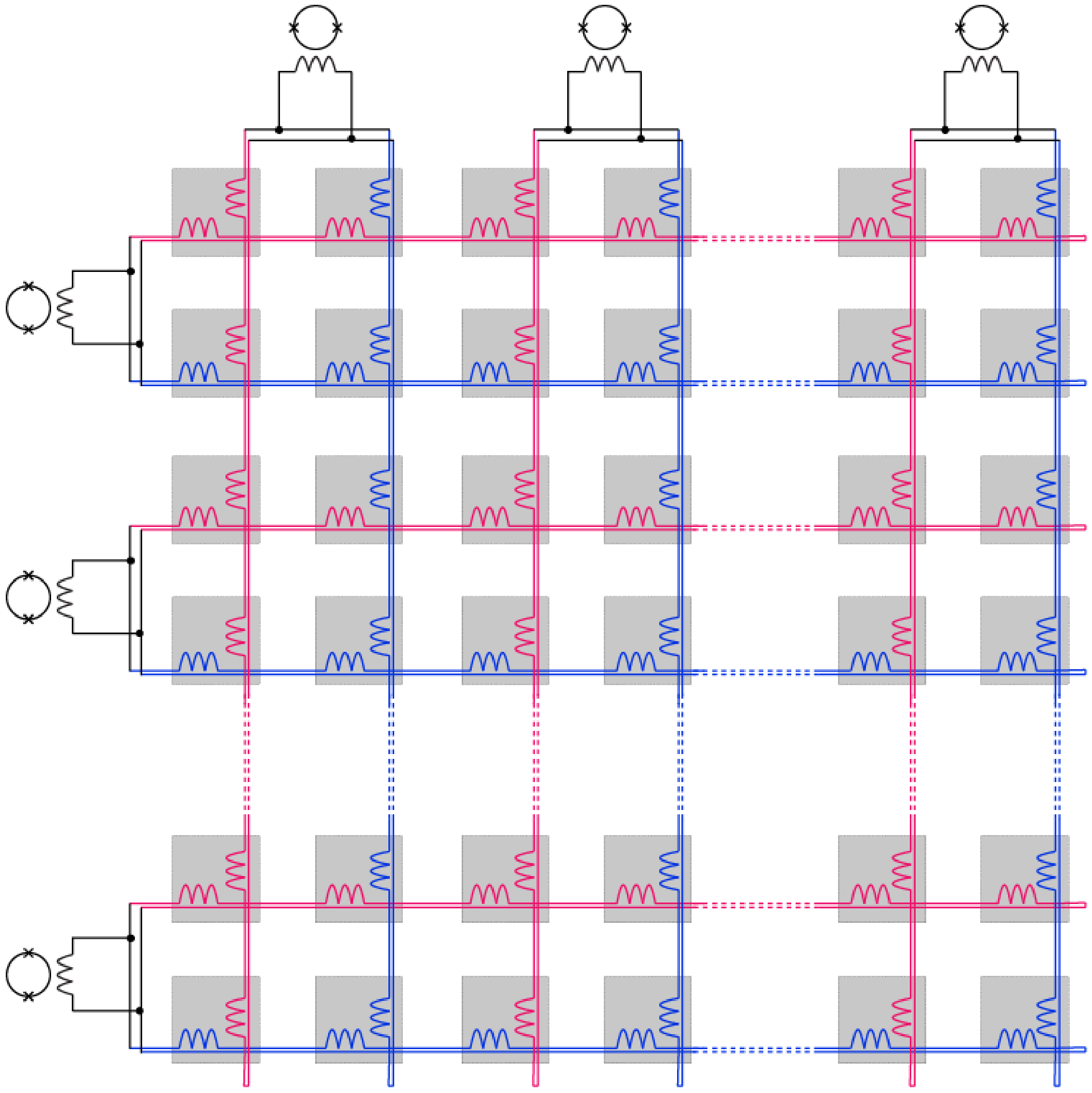

32 readout channels for 4000 pixels

1) The Hydra principle
2) Segmented sensor

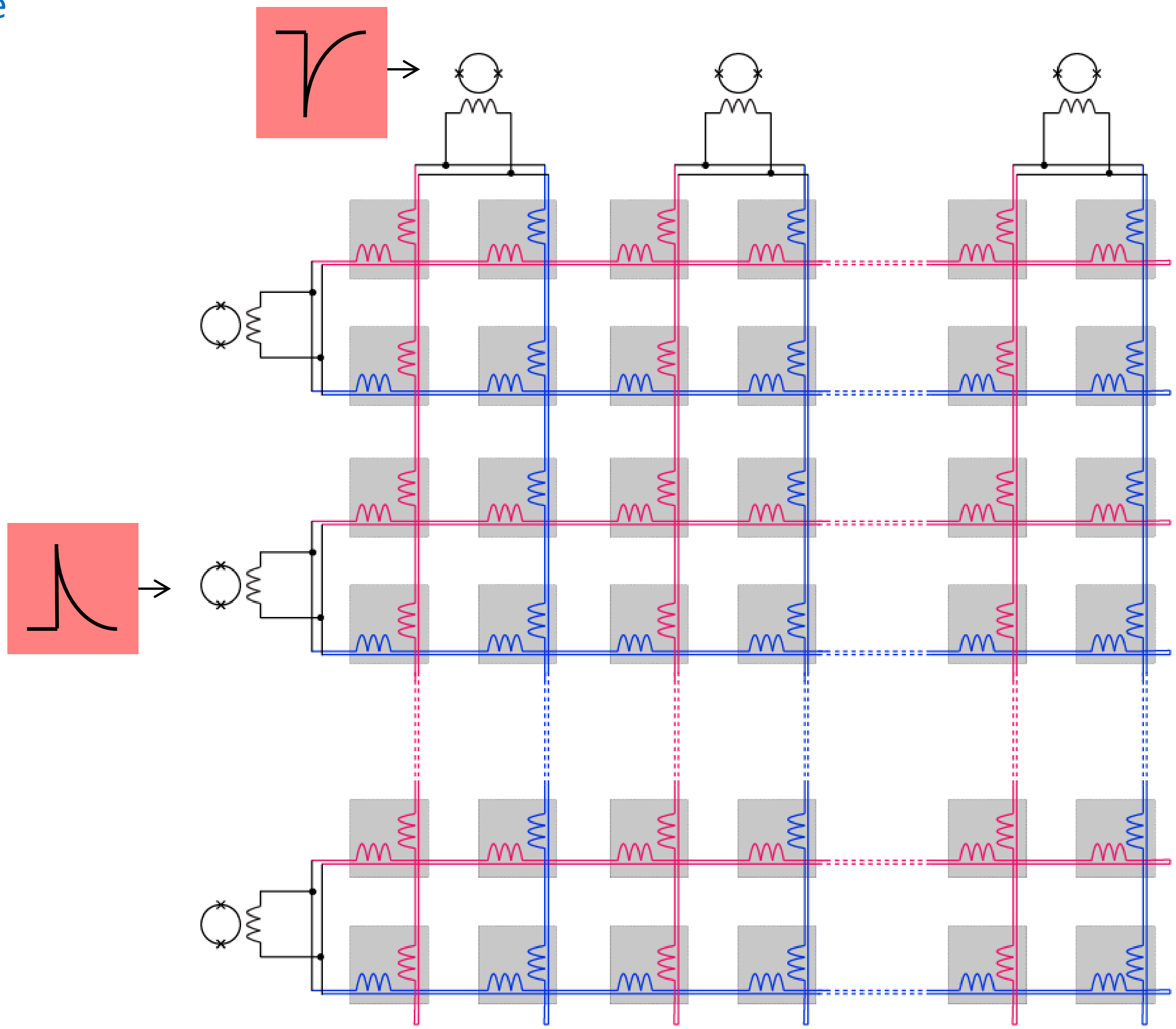

32 readout channels for 4000 pixels

1) The Hydra principle
2) Segmented sensor

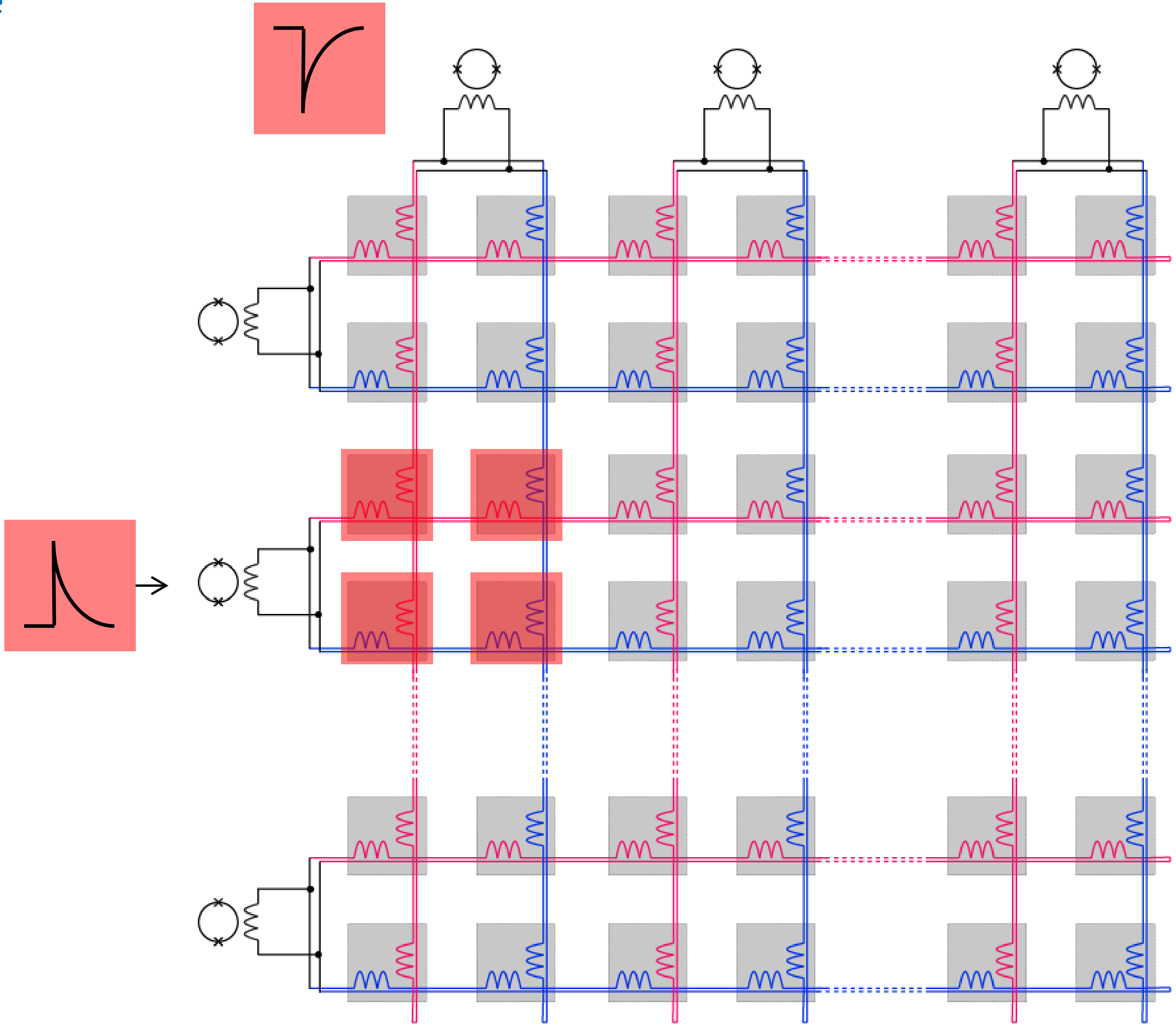

32 readout channels for 4000 pixels

1) The Hydra principle
2) Segmented sensor

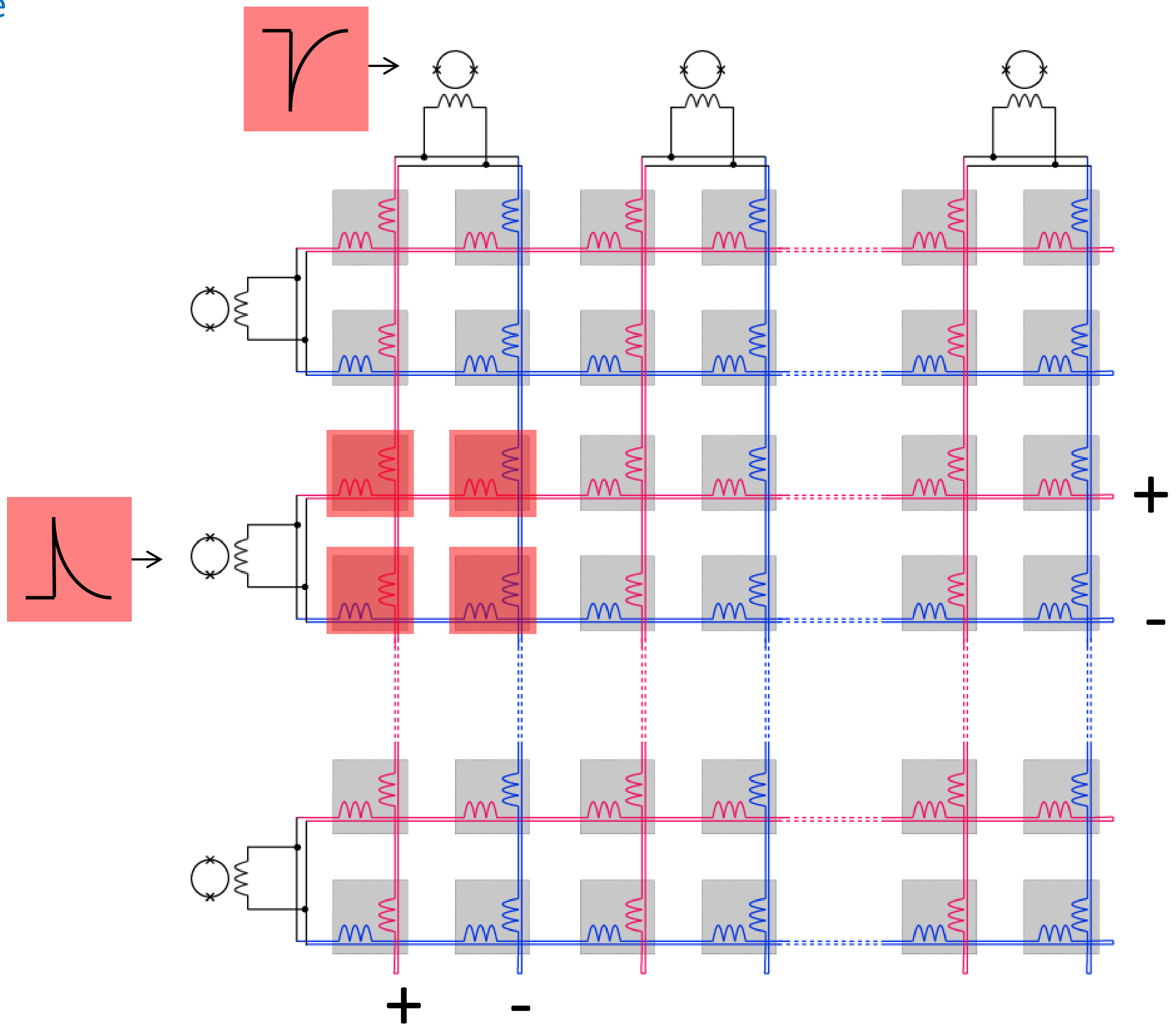

32 readout channels for 4000 pixels

1) The Hydra principle
2) Segmented sensor

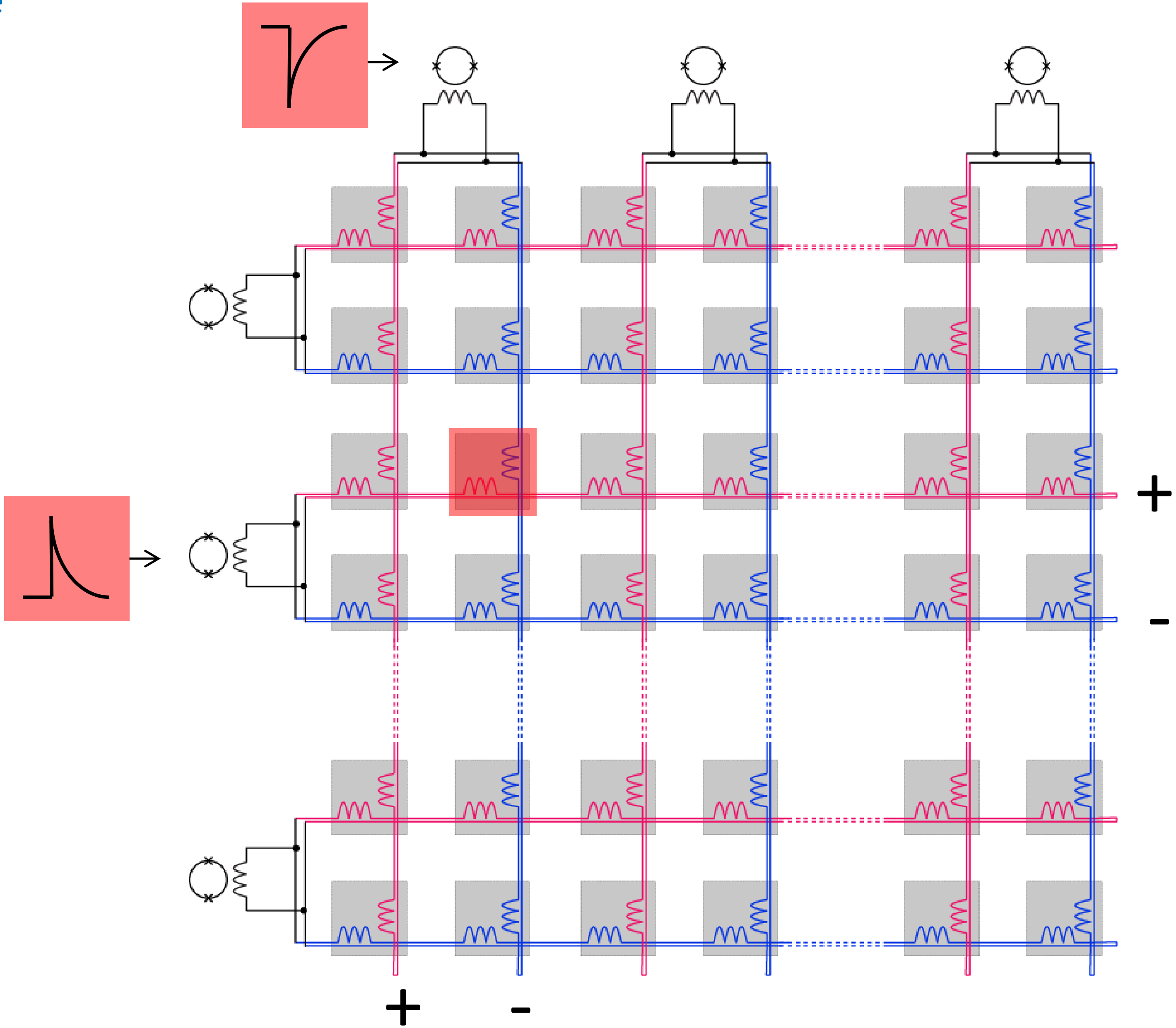

32 readout channels for 4000 pixels - MOCCA

1) The Hydra principle
2) Segmented sensor

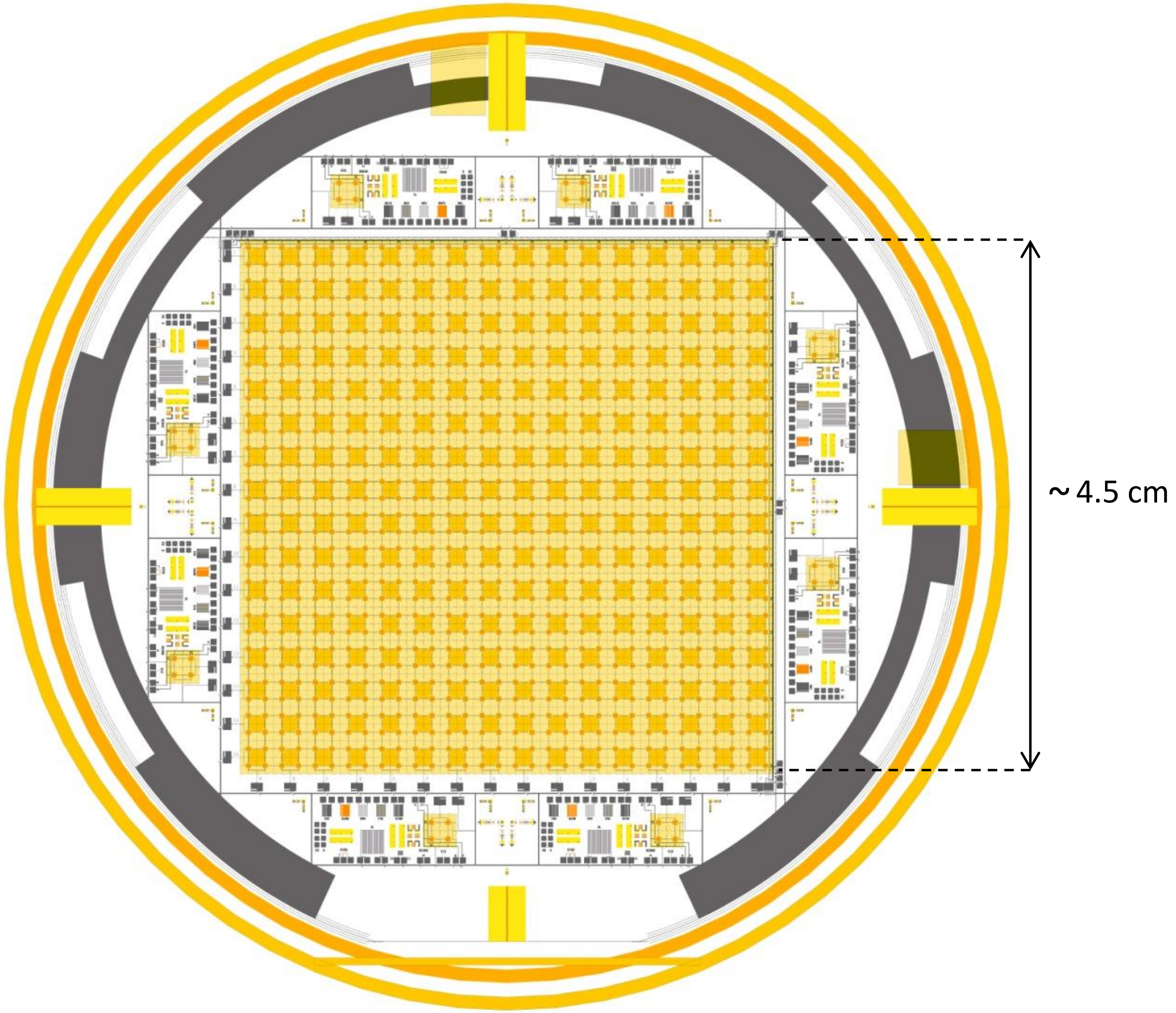

- 64 × 64 pixels
- ~100 eV (FWHM)
- 32 × 32 temperature sensors
- Read out by 16 + 16 SQUIDs

L. Gamer et al., *J. Low Temp. Phys.* **184** 839 (2016)

32 readout channels for 4000 pixels - MOCCA

1) The Hydra principle
2) Segmented sensor

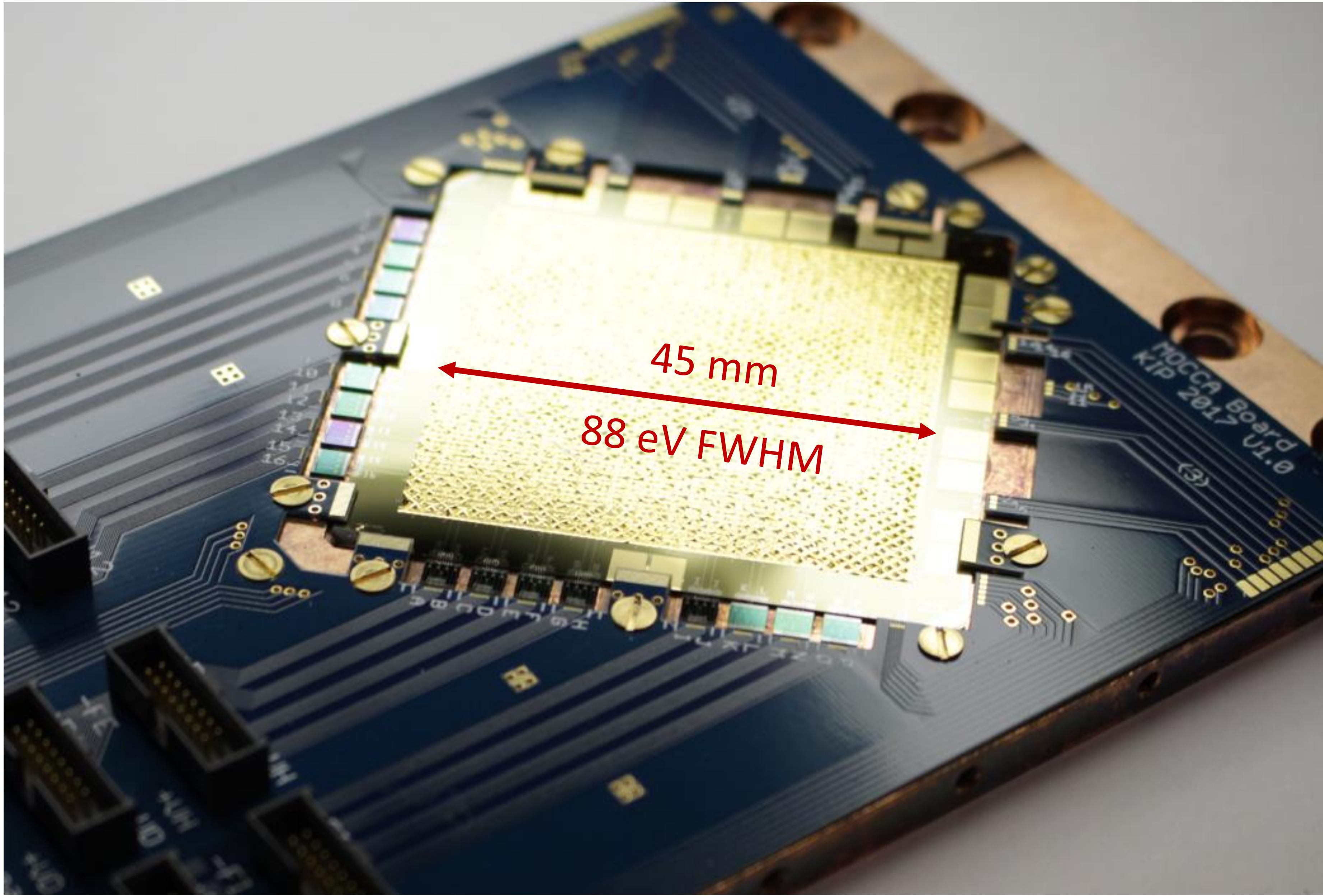

- 64×64 pixels
- ~100 eV (FWHM)
- 32×32 temperature sensors
- Read out by $16+16$ SQUIDs

MMCs for the ECHo experiment

The ECHo Collaboration *EPJ-ST* **226** 8 (2017) 1623

ECHo uses large arrays of MMCs with enclosed ^{163}Ho

$$^{163}_{67}\mathrm{Ho} \rightarrow ^{163}_{66}\mathrm{Dy}^{*} + \nu_{e}$$

$$^{163}_{66}\mathrm{Dy}^{*} \rightarrow ^{163}_{66}\mathrm{Dy} + E_{C}$$

Fraction of events in the last eV ~10^{-12}

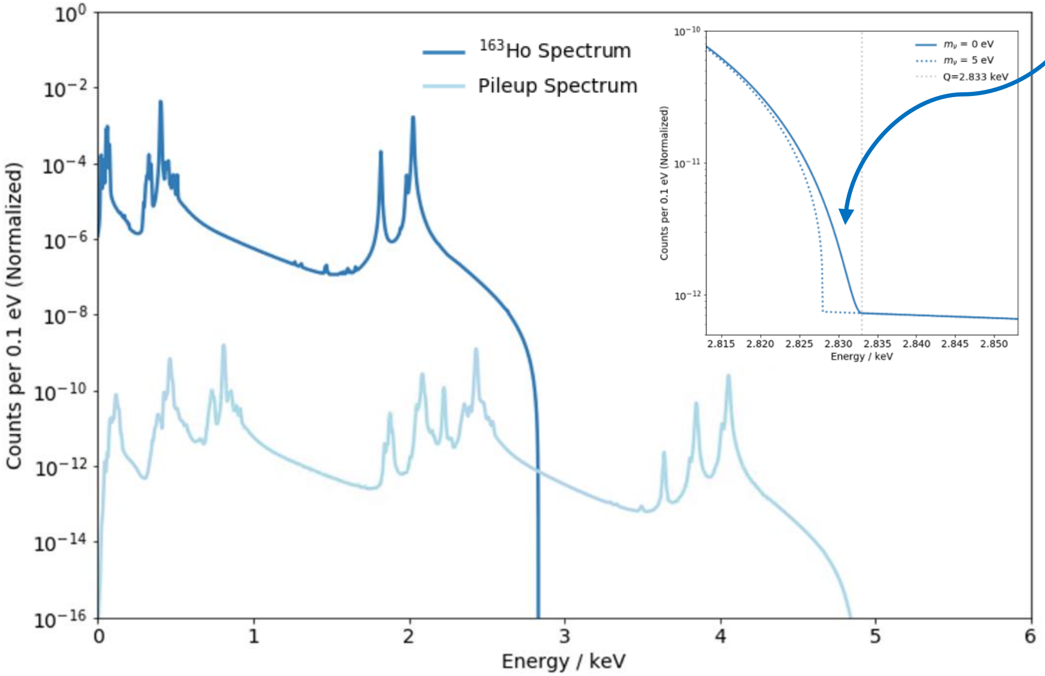

M. Braß and M. W. Haverkort, *New J. Phys.* **22** (2020) 093018

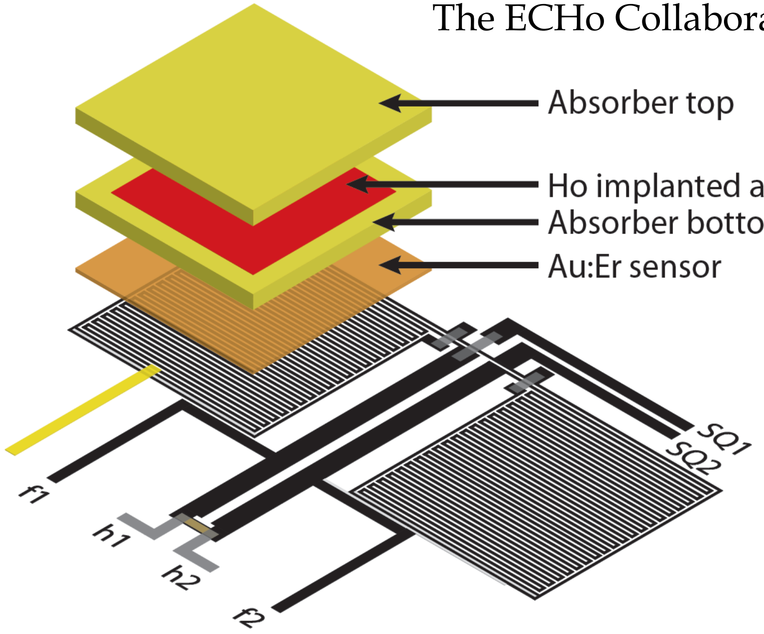

Implantation square: 150 µm x 150 µm

Second absorber: 165 µm x 165 µm

First absorber: 180 µm x 180 µm

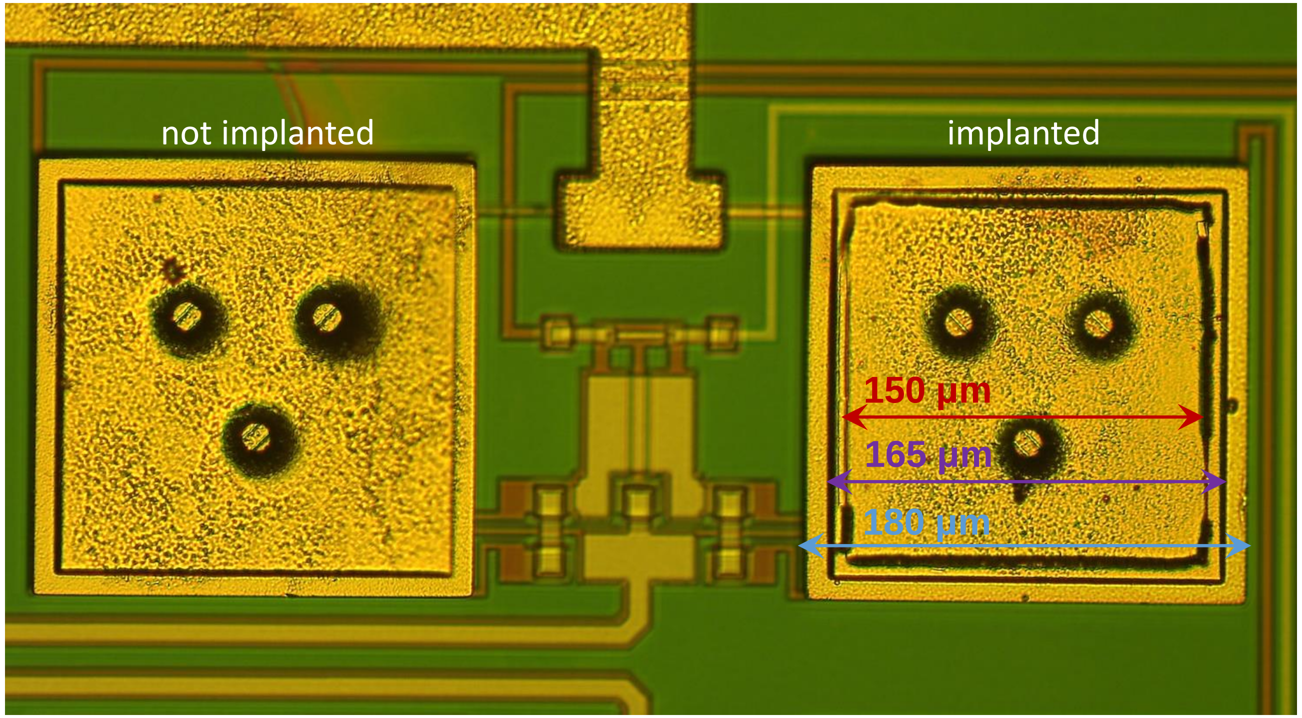

ECHo-1k array

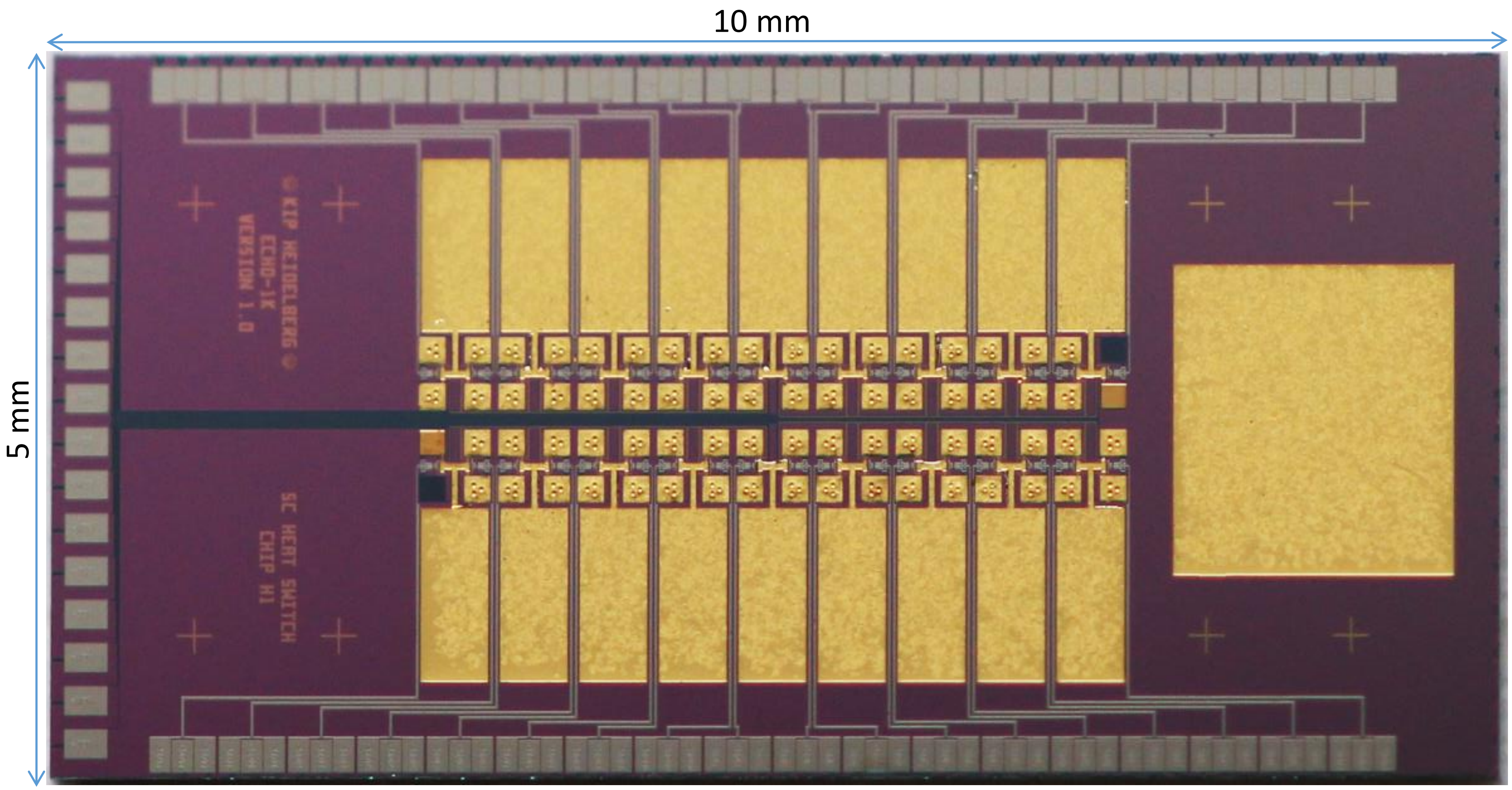

64 pixels can be loaded with ^{163}Ho
+ 2 temperature pixels
+ 2 detectors for diagnostics

Design performance:
ΔE_{FWHM} ~ 5 eV
τ_r ~ 90 ns (single channel readout)

F. Mantegazzini et al., NIM A, Vol. 1030, 2022, 166406

ECHo-1k array

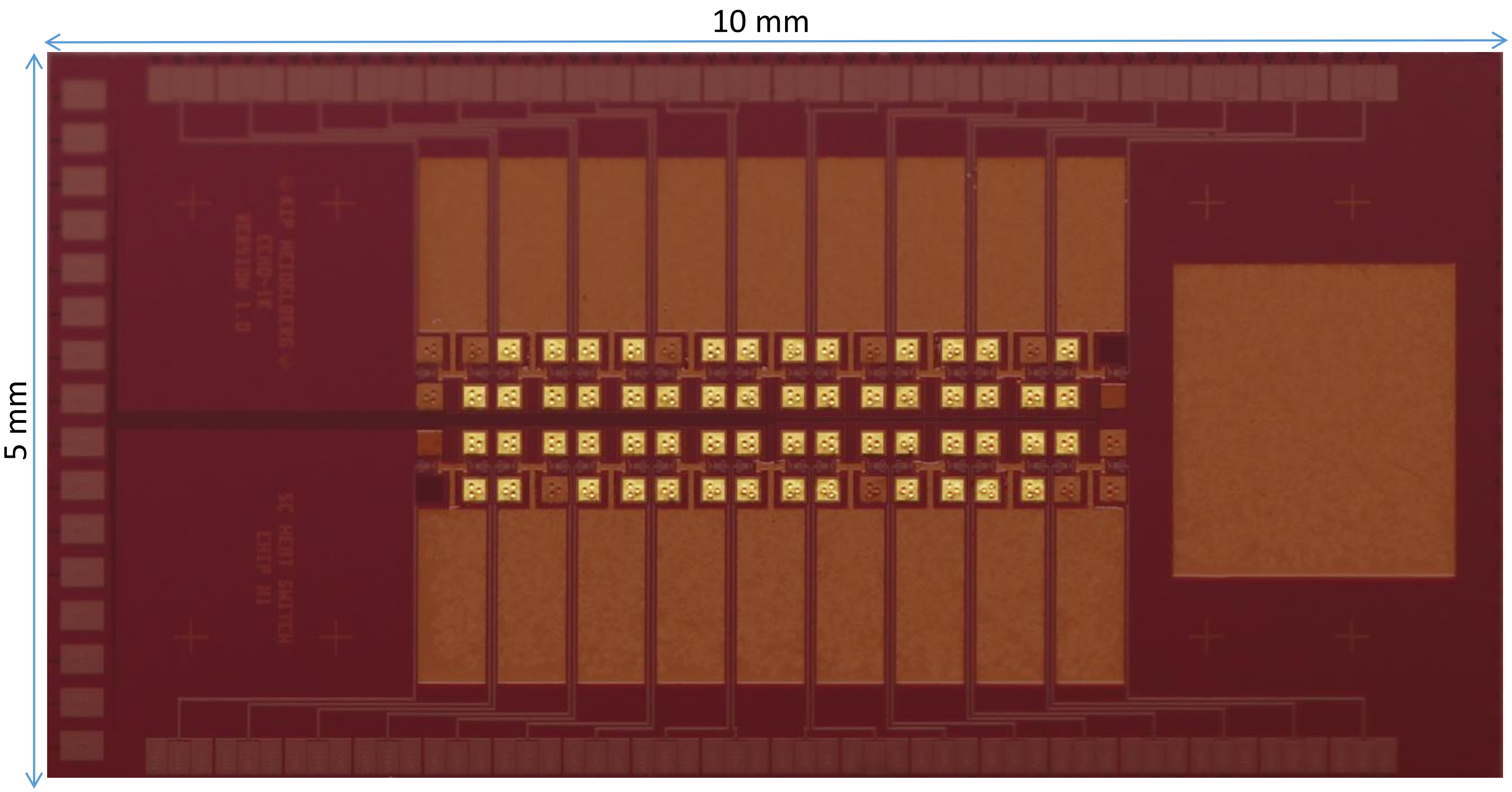

64 pixels can be loaded with ^{163}Ho
+ 2 temperature pixels
+ 2 detectors for diagnostics

Design performance:
ΔE_{FWHM} ~ 5 eV
τ_r ~ 90 ns (single channel readout)

✓ presence of non-implanted chips for in-situ background determination

F. Mantegazzini et al., NIM A, Vol. 1030, 2022, 166406

ECHo-1k readout

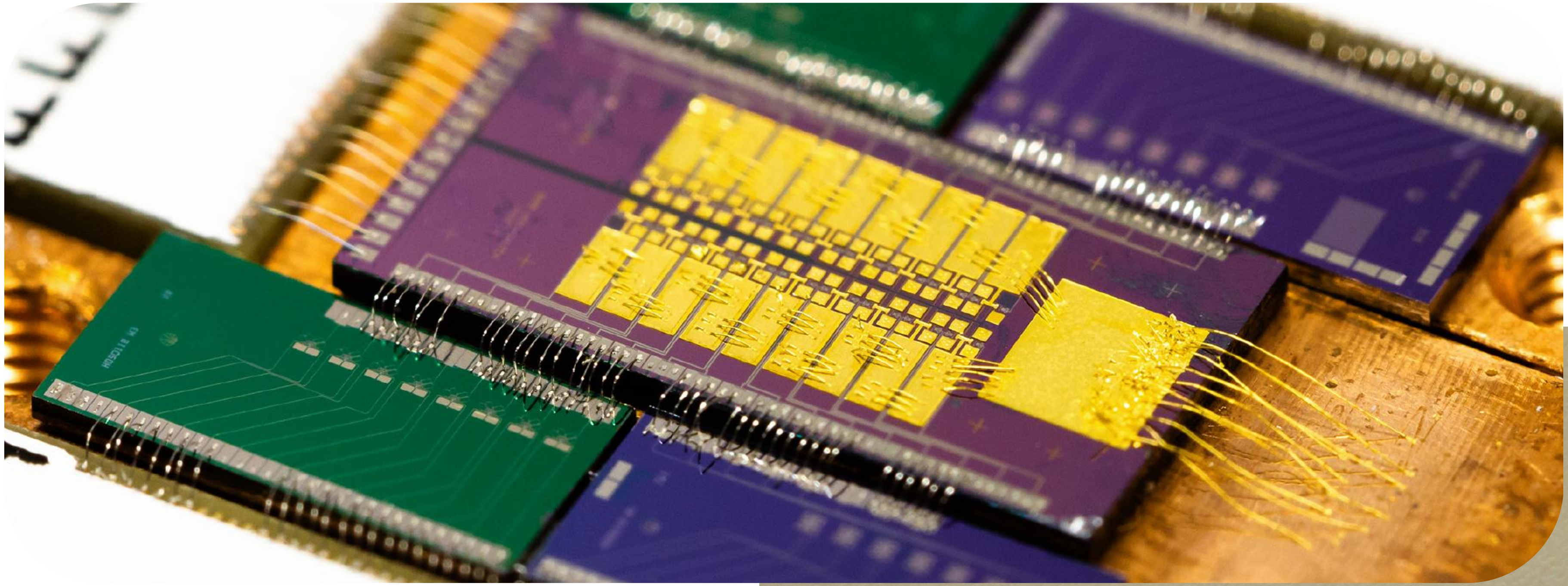

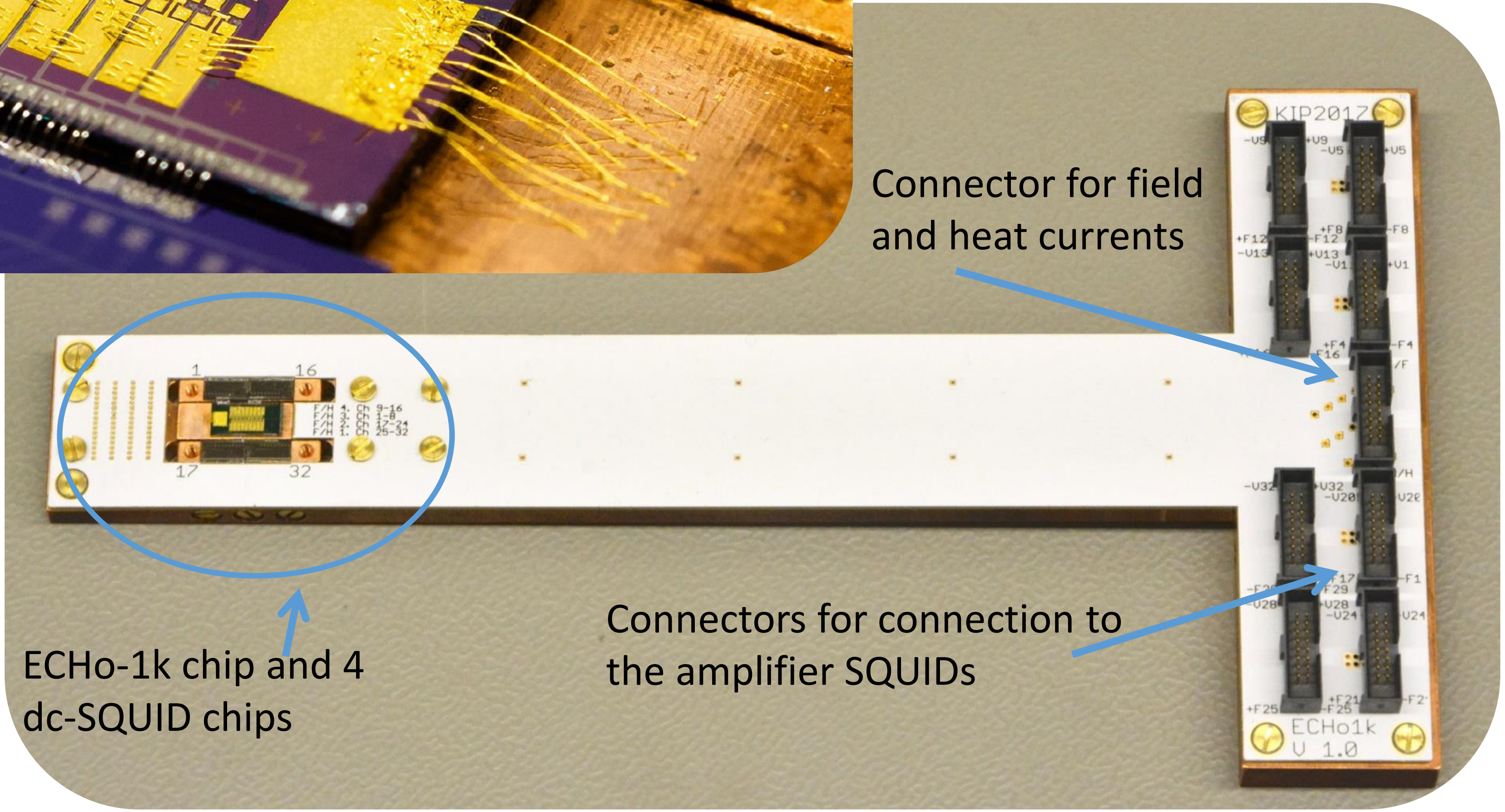

ECHo-1k chip-Au implanted @RISIKO

- High purity ^{163}Ho source
  → activity per pixel $a \approx 1$ Bq
- 4 Front-end chips each with 8 dc-SQUIDs for parallel readout

F. Mantegazzini et al., *JINST* **16** (2021) P08003

ECHo-1k data – Live!

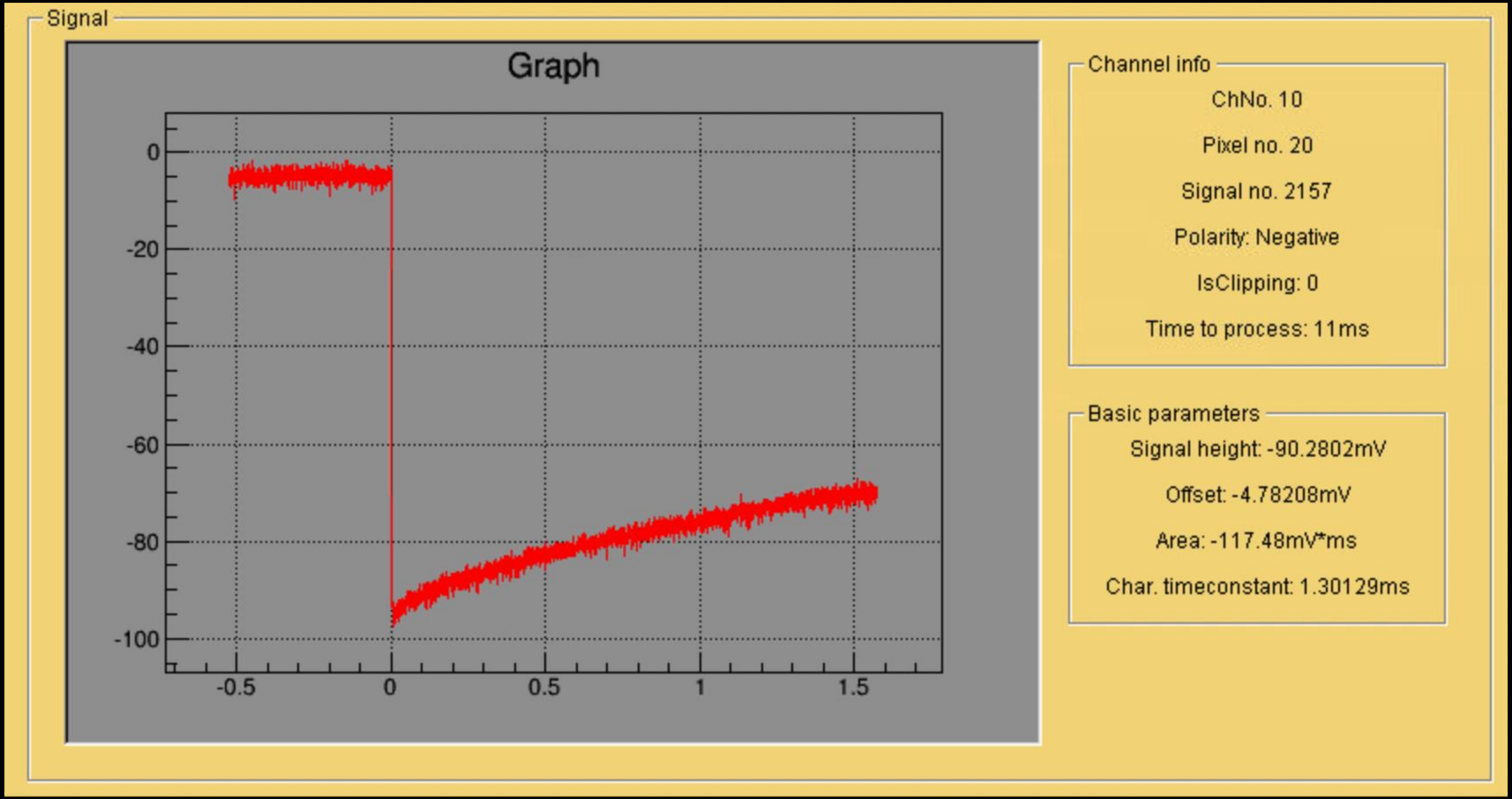

Data reduction

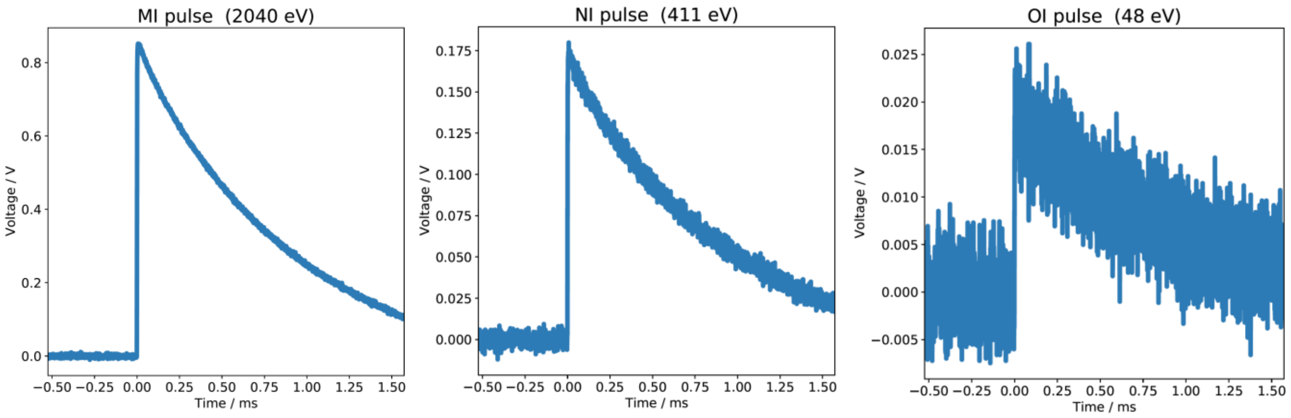

R. Hammann et al., *Eur. Phys. J. C* (2021) 81:963

Data reduction

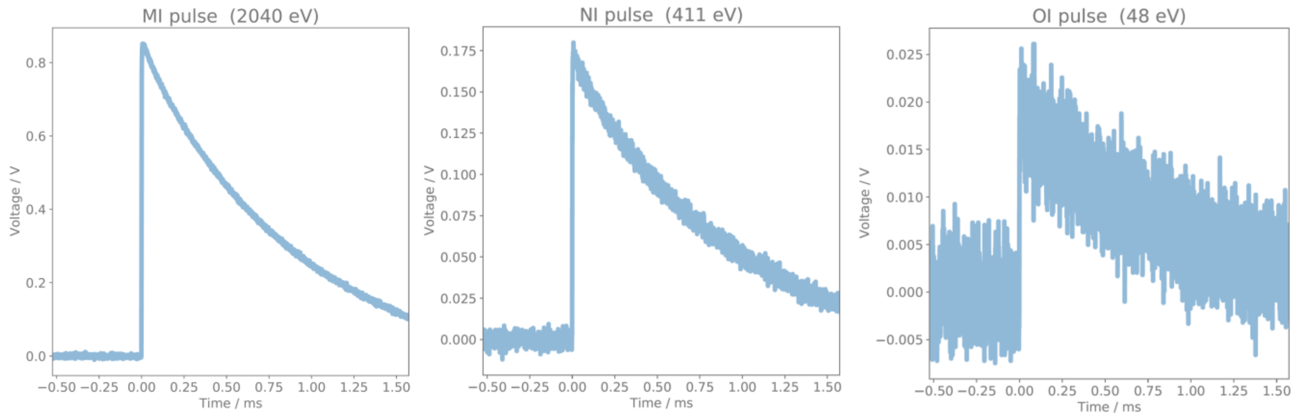

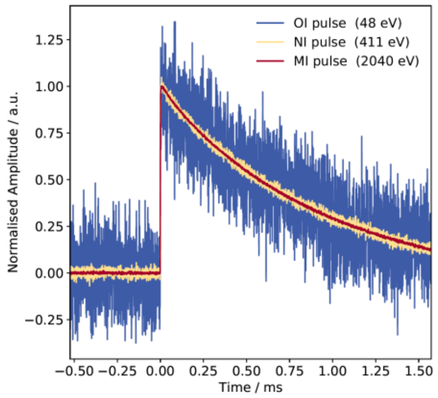

R. Hammann et al., *Eur. Phys. J. C* (2021) 81:963

Data reduction

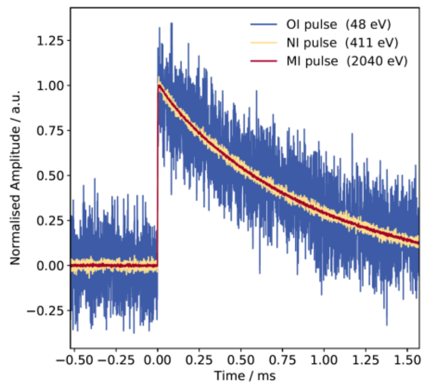

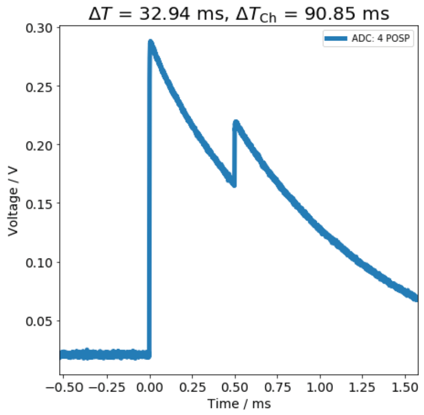

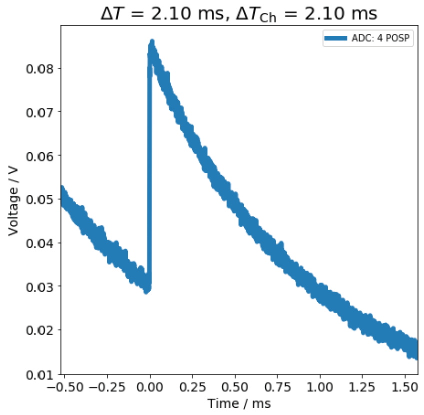

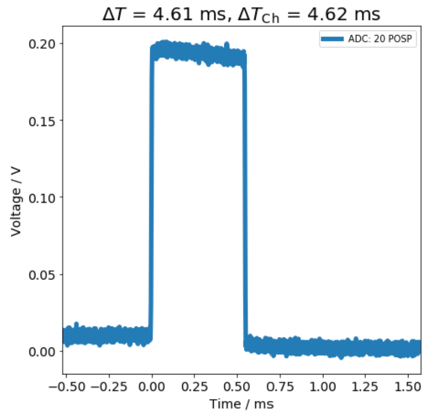

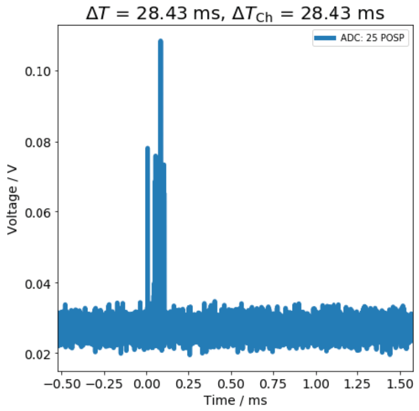

^{163}Ho events

Energy independent pulse shape

→ Pulse shape discrimination can be used to select ^{163}Ho Pulses

^{163}Ho pile-up events

in time window

→ pulse shape discrimination

outside the time window

→ trigger hold-off

Triggered noise

GSM signals

→ well-defined repetition time

electromagnetic signal coupled to readout

Muon related events + background events

R. Hammann et al., *Eur. Phys. J. C* (2021) 81:963

Data reduction - structure

- The acquisition of all channels is synchronized
- For each acquired trace, the trigger time is saved

→ ΔT_{Ch} Time difference to previous trace in a channel

→ ΔT Time difference to previous trace in any channel

First Level: Time Information Filter

Holdoff Filter

Discard traces with $\Delta T_{Ch} < T_{Holdoff}$

Burst Filter

Discard time intervals with abnormally high rate

Coincidence Filter

Discard traces with $\Delta T < T_{Coincidence}$

GSM Filter

Discard traces with ΔT associated to GSM pulse frequencies

Energy independent filter

Second Level:

Template Fit

- Create mean pulse from traces by cross-fitting traces in batches
- Fit traces to template to recover amplitude and χ_{red}^2

Pulse Shape Filter

Discard traces with high deviation from template

tiny and predictable energy dependence

Example

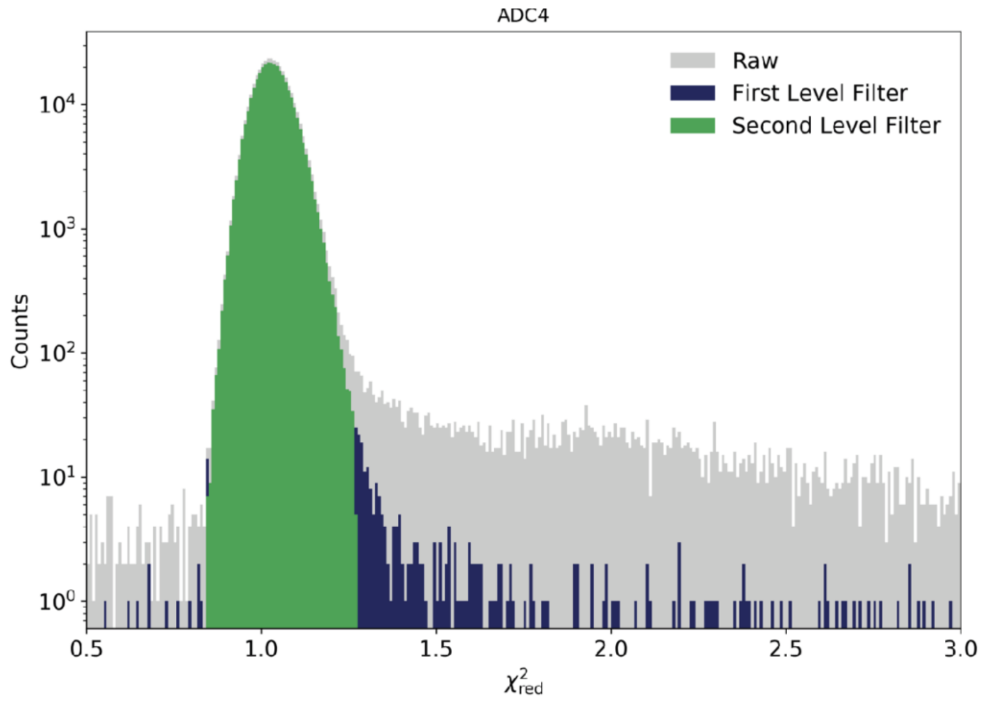

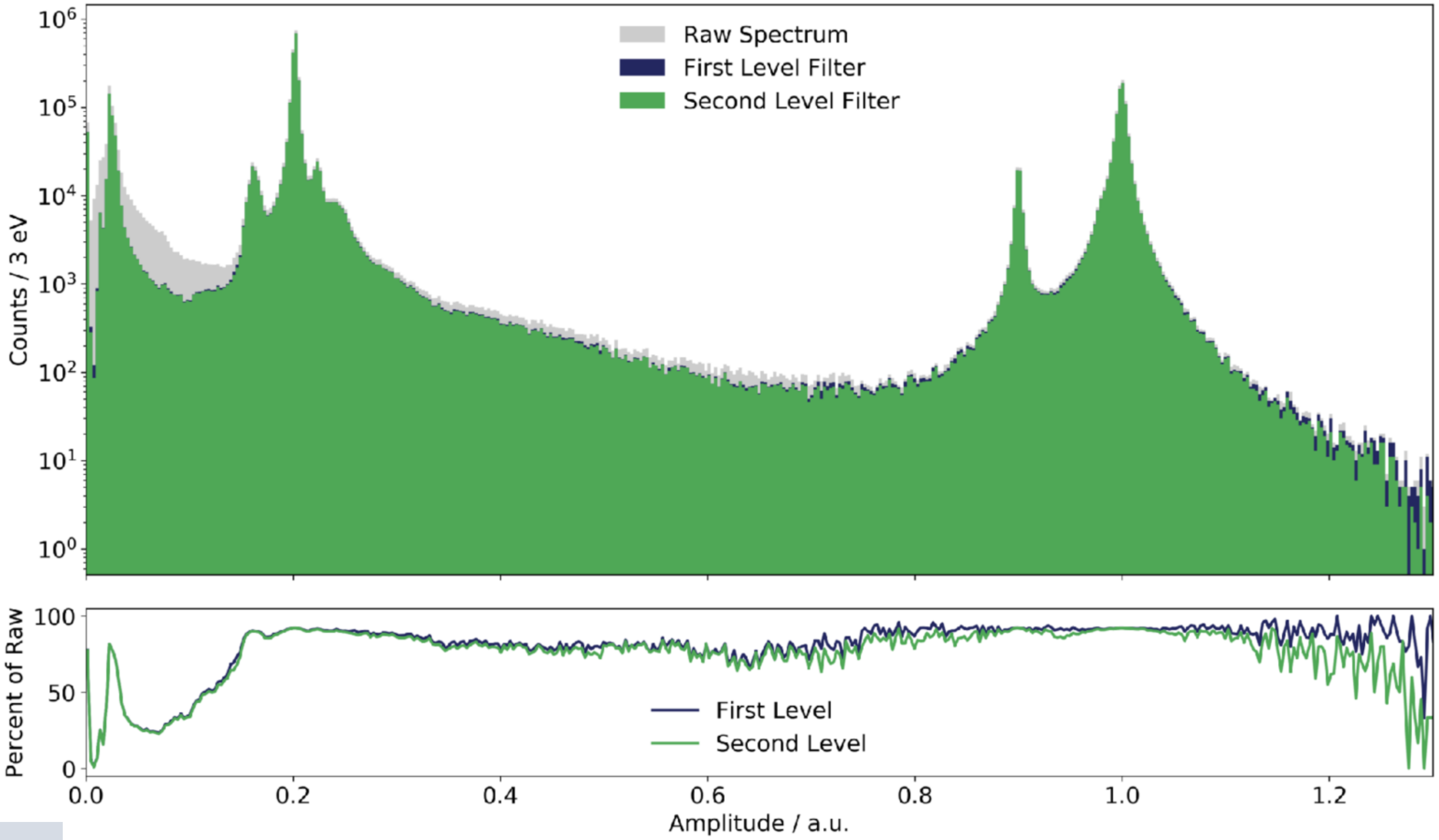

On-going:

- determination of efficiency for filters

R. Hammann et al., *Eur. Phys. J. C* (2021) 81:963

Combining many files

Quality checks

1. level filter
Monitor fraction of removed events over time for a pixel

2. level filter
Monitor χ^2 distribution

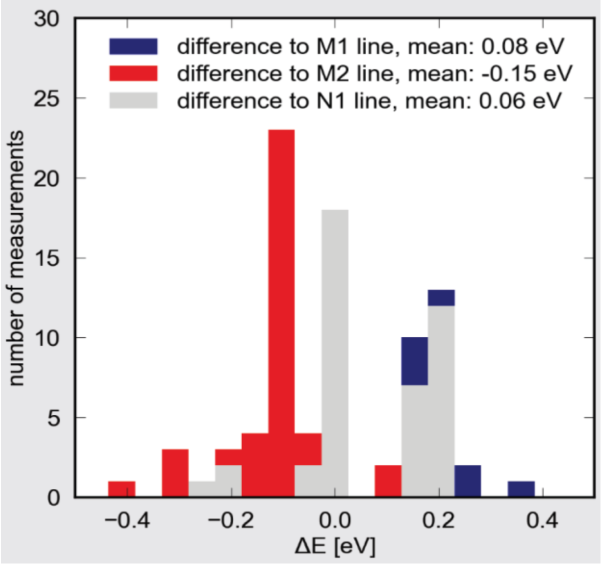

Energy calibration
new calibration with ^{55}Fe with a ^{163}Ho high resolution spectrum
→ Alignment test

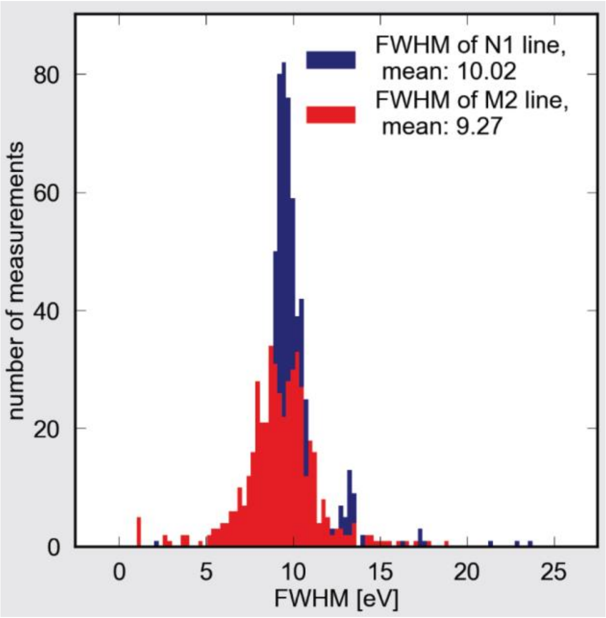

Energy resolution
Extract “Pseudo-energy resolution” for each single histogram
→ define acceptance range

Conclusions

metallic magnetic calorimeters

- are versatile low temperature detectors
- high resolution for all kinds of particles
- wide range of energies
- impressive resolving power

micro-farbrication works

- detector arrays reliably fabricated
- designed performance is reached
- reproducibility of performance

multiplexing

- demonstrated principles

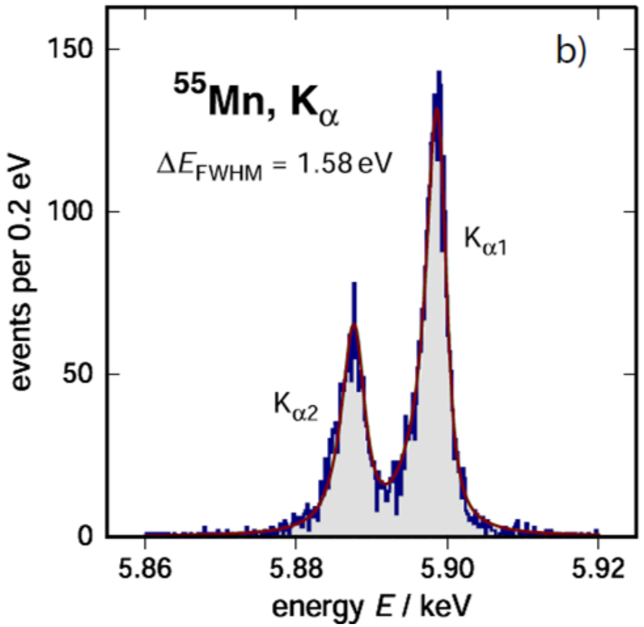

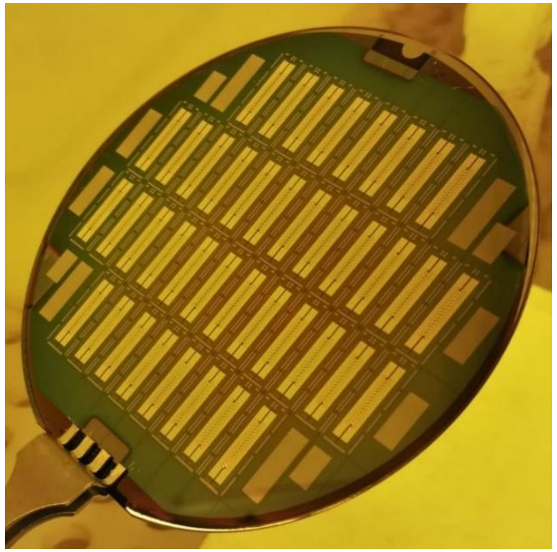

Conclusions

metallic magnetic calorimeters

- are versatile low temperature detectors
- high resolution for all kinds of particles
- wide range of energies
- impressive resolving power

micro-farbrication works

- detector arrays reliably fabricated
- designed performance is reached
- reproducibility of performance

multiplexing

- demonstrated principles

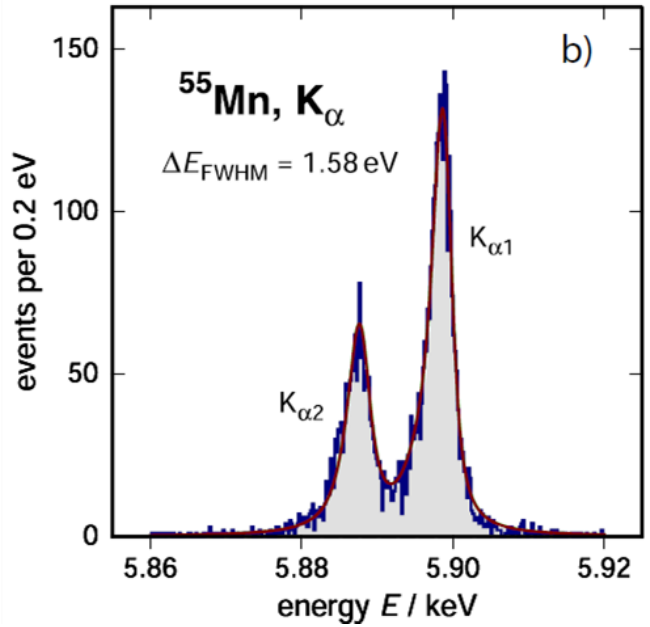

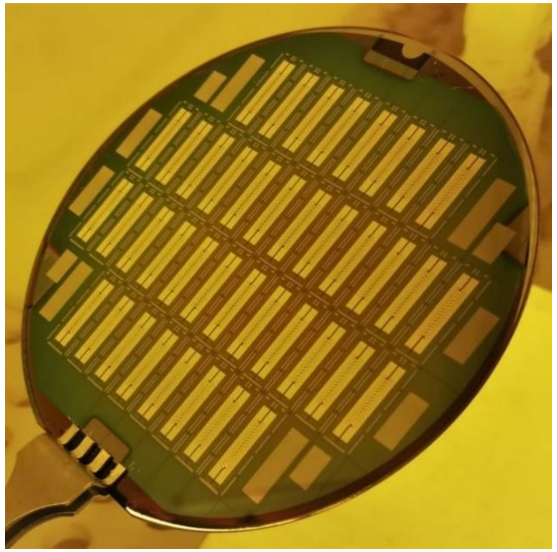

Thank you for the attention!